Polarized Lung Inflammation and Tie2/Angiopoietin-Mediated Endothelial Dysfunction during Severe *Orientia tsutsugamushi* Infection

Running title: Pulmonary inflammatory mediators in severe scrub typhus

Brandon Trent[1], Yuejin Liang[2], Yan Xing[2, #a], Marisol Esqueda[2], Yang Wei[2, #b], Nam-Hyuk Cho[3,4], Hong-Il Kim[4], Yeon-Sook Kim[5], Thomas R. Shelite[2,#c], Jiyang Cai[6, #d], Jiaren Sun[1,2], Donald H. Bouyer[1], Jinjun Liu[7,*], Lynn Soong[1,2,*]

[1]Department of Pathology, University of Texas Medical Branch, 301 University Blvd, Galveston, TX 77555-0609

[2]Department of Microbiology and Immunology, University of Texas Medical Branch, 301 University Blvd, Galveston, TX 77555-1070

[3]Department of Microbiology and Immunology, Seoul National University College of Medicine, Seoul 03080, Republic of Korea

[4]Department of Biomedical Sciences, Seoul National University College of Medicine, Seoul 03080, Republic of Korea

[5]Division of Infectious Diseases, Department of Internal Medicine, Chungnam National University School of Medicine, Daejeon 35015, Republic of Korea

[6]Department of Ophthalmology & Visual Sciences, University of Texas Medical Branch, Galveston, 301 University Blvd., Galveston, TX 77555-1106

[7]Department of Physiology and Pathophysiology, School of Basic Medical Sciences, Xi'an Jiaotong University Health Science Center, Xi'an 710061, China

[#a]Current Address: People's Hospital of Henan Province, Henan 450003, China

[#b]Current Address: Core Research Laboratory, The Second Affiliated Hospital of Xi'an Jiaotong University, Xi'an 710004, China

[#c]Current Address: Department of Internal Medicine, Division of Infectious Diseases, University of Texas Medical Branch, 301 University Blvd, Galveston, TX 77555-0435

[#d]Current Address: Department of Physiology, OUHSC, 940 Stanton Young Blvd., Oklahoma City, OK 73104-5042

[*] Corresponding Authors: Jinjun Liu: jupet@163.com; Lynn Soong: lysoong@utmb.edu

Key Words: *Orientia tsutsugamushi,* endothelial cell, Tie2, angiopoietin, macrophage

Abstract

Orientia tsutsugamushi infection can cause acute lung injury and high mortality in humans; however, the underlying mechanisms are unclear. Here, we tested a hypothesis that dysregulated pulmonary inflammation and Tie2-mediated endothelial malfunction contribute to lung damage. Using a murine model of lethal *O. tsutsugamushi* infection, we demonstrated pathological characteristics of vascular activation and tissue damage: 1) a significant increase of ICAM-1, VEGFR2, and angiopoietin-2 (Ang2) proteins in inflamed tissues and lung-derived endothelial cells (EC), 2) a progressive loss of endothelial quiescent and junction proteins (Ang1, VE-cadherin/CD144, occuludin), and 3) a profound impairment of Tie2 receptor at the transcriptional and functional levels. *In vitro* infection of primary human EC cultures and serum Ang2 proteins in scrub typhus patients support our animal studies, implying endothelial dysfunction in severe scrub typhus. Flow cytometric analyses of lung-recovered cells further revealed that pulmonary macrophages (MΦ) were polarized toward an M1-like phenotype ($CD80^+CD64^+CD11b^+Ly6G^-$) during the onset of disease and prior to host death, which correlated with the significant loss of $CD31^+CD45^-$ ECs and M2-like ($CD206^+CD64^+CD11b^+Ly6G^-$) cells. In vitro studies indicated extensive bacterial replication in M2-type, but not M1-type, MΦs, implying the protective and pathogenic roles of M1-skewed responses. This is the first detailed investigation of lung cellular immune responses during acute *O. tsutsugamushi* infection. It uncovers specific biomarkers for vascular dysfunction and M1-skewed inflammatory responses, highlighting future therapeutic research for the control of this neglected tropical disease.

Author Summary

Scrub typhus is a life-threatening disease, infecting an estimated one million people yearly. Acute lung injury is the most common clinical observation; however, its pathogenic biomarkers and mechanisms of progression remain unknown. Here, we used a lethal infection mouse model that parallels certain aspects of severe scrub typhus, primary human endothelial cell cultures, and patient sera to define pathogenic biomarkers following *Orientia tsutsugamushi* infections. We found a significant increase in the levels of endothelial activation/stress markers (angiopoietins and ICAM-1) in infected mouse lungs and in patient sera, but a progressive loss of endothelium-specific Tie2 receptor and junction proteins (VE-cadherin), at severe stages of disease. These signs of vasculature disruption positively correlated with the timing and magnitude of recruitment/activation of proinflammatory MΦ subsets in infected lungs. Bacterial growth *in vitro* was favored in M2-like, but not in M1-like, MΦs. This study, for the first time, reveals endothelial malfunction and dysregulated inflammatory responses, suggesting potential therapeutic targets to ameliorate tissue damage and pathogenesis.

74 # Introduction

75 Scrub typhus is a febrile and potentially lethal illness that infects an estimated one million
76 individuals per year [1]. The disease is caused by infection with the bacterium, *Orientia*
77 *tsutsugamushi*. Nearly a third of the human population lives in endemic areas, known as the
78 "tsutsugamushi triangle", although recent reports have identified scrub typhus in South America,
79 which was previously believed to be free of scrub typhus [1, 2]. Within endemic areas, scrub
80 typhus is reported to cause a substantial proportion (approximately 15-23%) of reported febrile
81 illness [3, 4]. If left untreated, scrub typhus can manifest as interstitial pneumonia, myocardial
82 and hepatic inflammation, and meningoencephalitis. [5]. Mild interstitial pneumonitis is typically
83 the extent of pulmonary involvement during self-resolving or promptly treated scrub typhus.
84 However, life-threatening pathologies can arise in severe cases, including lung hemorrhage,
85 edema buildup, diffuse alveolar damage, and interstitial cellular infiltration [6]. Acute respiratory
86 distress syndrome and lung damage are associated with high mortality and present in 6.75-25%
87 of scrub typhus patients [5, 7]; however, there is no detailed investigation of the underlying
88 mechanisms responsible for pulmonary endothelial dysfunction and inflammation.
89
90 Being an obligate intracellular bacterium, *O. tsutsugamushi* can infect a variety of host cells but
91 primarily replicate in macrophages (MΦs)[8], dendritic cells [9], and endothelial cells (ECs) [6,
92 8]. The bacteria enter host cells via the phagosome [10] or endosome [11], which they
93 subsequently escape to begin replication in the cytoplasm. Infection-triggered cellular responses,
94 including the activation of activator protein-1 (AP-1) and NF-κB pathways, the production of
95 proinflammatory cytokines (IL-1β, TNF-α, IL-8/CXCL8), and the expression of distinct gene
96 profiles, have been examined *in vitro* by using primary human umbilical vein endothelial cells

(HUVEC) [12], human epithelial/EC-like ECV304 cell line [13], human monocytes or MΦs [14]. Prolonged infection can result in EC death via apoptosis [15], but there is limited information on endothelial responses during the course of *O. tsutsugamushi* infection [16]. Sublethal *O. tsutsugamushi* infection studies in outbred Swiss CD-1 mice [17], as well as clinical studies of human patients [18], have shown significant elevation of endothelial activation markers (ICAM-1, VCAM-1, E-Selectin, etc.) in the serum of infected individuals; however, endothelium-focused analyses during *in vivo* infection remain largely unexplored. Several studies have characterized the response and activation of MΦs during *O. tsutsugamushi* infection [19, 20]. *In vitro* and *ex vivo* experiments have shown that human monocytes/MΦs in the circulation adopt an inflammatory "M1" type transcriptional profile after *O. tsutsugamushi* infection, although little is known regarding tissue specific macrophages or the presence of alternatively activated "M2"-type macrophages [21].

The delicate balance of EC quiescence and activation is crucial during systemic infection. While EC activation promotes adherence and recruitment of innate and adaptive immune cells for pathogen clearance, prolonged activation can lead to EC cytotoxicity, impaired barrier function, and host mortality [22]. One of the critical mechanisms to control EC activation status and cellular function is through competitive interactions between angiopoietin-1 (Ang1) and Ang2 ligands with their receptor, Tie2, a protein tyrosine kinase that is predominately expressed on ECs in humans and mice. Tie2 activation and phosphorylation via binding with Ang1 (produced by pericytes and platelets [23]) promote EC quiescence, which limits leukocyte adhesion and maintains EC survival and vascular barrier integrity [24]. Infection- or inflammation-triggered release of Ang2 (normally stored within the Weibel-Palade bodies in ECs [25, 26]) can compete

120 with Ang1 binding Tie2 to antagonize its function [27]. Inhibition of Tie2 signaling via Ang2
121 binding stimulates leukocyte adhesion, vascular barrier destabilization, and inflammation [28,
122 29]. Thus, Ang2/Ang1 expression ratios and Tie2 activation status are important biomarkers for
123 the pathogenesis of systemic infection, such as severe sepsis and malaria [30, 31].
124
125 To investigate endothelial alterations during severe *O. tsutsugamushi* infection, we have recently
126 developed a lethal intravenous *O. tsutsugamushi* infection model in C57BL/6 mice [32-34],
127 which parallels aspects of severe scrub typhus in humans. In our lethal models, bacterial loads in
128 both the spleen and liver reached peak levels around or shortly after the onset of disease (days 6-
129 8 post-infection), and are reduced significantly by days 10-12. In contrast, lung bacterial loads
130 remain elevated throughout infection [35]. All mice expire by days 12-13, suggesting unknown
131 mechanisms of pathogenesis are at work during late infection [32, 35]. Given that the lungs are a
132 major organ for *O. tsutsugamushi* infection in humans and in different animal models, and that
133 elevated ratios of *ANG2/ANG1* transcripts are pathological hallmarks in lethal infection models
134 [32, 35], we hypothesize that dysregulated pulmonary inflammation and Tie2/Ang2-mediated
135 endothelial dysfunction contribute to disease pathogenesis at late stages of *O. tsutsugamushi*
136 infection.
137
138 In this study, we utilized a lethal infection model in C57BL/6 mice, *in vitro* infection systems
139 (human EC cultures, and bone marrow-derived MΦ subsets), as well as sera from scrub typhus
140 patients to reveal positive correlations between vascular dysfunction, activation of innate
141 immune cells, and disease progression. We focused on two cellular subsets known to be sites of
142 *O. tsutsugamushi* replication, ECs and MΦs, to characterize their activation and polarization *in*

143 *vivo*. To the best of our knowledge, this is the first report to delineate MΦ subsets in inflamed
144 lungs and their positive correlation with Tie2 malfunction during late stages of severe infection.
145

Results

Pulmonary EC activation and tight junction disruption during infection in mice

Given that the lung is a major site of *O. tsutsugamushi* infection in humans and animal models [6, 32] and that EC activation and disruption of vascular barrier integrity are principal steps for acute lung injury in sepsis and pneumonia models [36], we sought to investigate pulmonary EC activation in C57BL/6 mice following i.v. inoculation with a lethal dose of *O. tsutsugamushi* Karp (~1.325×10^6 viable bacteria in 200 µl of PBS). Inoculation via this route establishes bacterial replication in the lungs accompanied by interstitial pneumonitis and alveolar thickening (S1A Fig, [35]). Immunofluorescent staining of frozen lung sections revealed increased ICAM-1-positive (green) vascular staining on days 2 (D2) to 9, as well as a close association of bacterial (red) with activated endothelium at D9 (Fig 1A, boxed area, Fig 1C). To examine endothelial structure and adherens junctions, we co-stained lung sections with GSL I-B_4 lectin (specific for α-galactose residues known to be enriched on the surface of EC) and anti-VE-cadherin/CD144 (an adherens junction protein, red), as described in our previous report for neuroinflammation [34]. The VE-cadherin staining was intense and homogenous in the control tissues, but markedly reduced in D2 samples; VE-cadherin staining was nearly absent in some foci of D6 and D9 samples (Fig 1B-C), implying the reduction of junction proteins. In conjunction with the endothelial junction proteins, we co-stained the epithelial junction protein, occludin, and GSL I-B_4 lectin. Consistently, we found a progressive loss of occludin staining on the bronchial epithelium during the infection and a near absence of staining in D9 samples (S1B Fig). These data suggest a progressive and severe loss of vascular barrier integrity in the infected lungs, especially at late stages of acute infection prior to host death (D9) [32].

To support our immunofluorescent results, we prepared single-cell suspensions from mouse lung tissues and used flow cytometry to examine the frequency of recovered $CD31^{+}CD45^{-}$ ECs and their surface ICAM-1 expression. We found that compared with the mock controls, infected lung tissues contained a significant increase in the frequencies of $ICAM\text{-}1^{+}CD31^{+}CD45^{-}$ ECs at D6 and D9, respectively ($p < 0.001$, $p < 0.01$, Fig 1D), while there were approximately 5-folds reduction in the frequencies of total ECs at D6 and D9 ($p < 0.001$, S1C Fig). We also examined EC expression of vascular endothelial growth factor receptor 2 (VEGFR2), a critical factor controlling vascular permeability and barrier function [37]. Compared with the mock controls, there was an approximately 6-fold increase in the frequencies of $VEGFR2^{+}CD31^{+}CD45^{-}$ ECs in the lung tissues at D6 and D9 (Fig 1D). These flow cytometry data reinforced the immunofluorescent results, indicating marked endothelial activation and damage at D6 (the onset of disease) and D9 (prior to host demise). To validate these findings in mice, we infected primary HUVEC cultures with different doses of *O. tsutsugamushi* (3 and 10 MOI) and found a dose-dependent increase in *ICAM1* and *IL8/CXCL8* transcripts at 24 h post-infection (S1D Fig). Collectively, these data indicate infection-triggered endothelial stress and activation, accompanied by progressive vascular damage and tight junction disruption during the course of infection.

Alterations in the angiopoietin-Tie2 system during *Orientia* infection

Currently, there are no detailed *in vivo* studies to define molecular mechanisms underlying *O. tsutsugamushi* infection-associated vascular damage. For other severe and systemic infections caused by bacteria or viruses, alterations in angiopoietin proteins or their functional Tie2

192 receptor is considered as one of the key mechanisms for vascular dysfunction [38, 39] . Given
193 our previous findings of elevated *ANG2/ANG1* mRNA ratios in mice with severe scrub typhus
194 and in *O. tsutsugamushi*-infected HUVECs [33], we speculated that impairment in Tie2 function
195 occurs in severe scrub typhus [16]. To test this hypothesis, we examined Ang1, Ang2, and Tie2
196 protein levels in the lung tissues via immunofluorescent staining (Figs 2-3). While the mock
197 controls contained relatively high levels of Ang1 (green), with relatively low levels of Ang2
198 (red), we found a modest decrease in Ang1-positive staining but a steady increase in Ang2
199 staining, during the course of infection (Fig 2A). These IFA results were quantified,
200 demonstrating the significant decrease of Ang1 and a significant increase of Ang2 expression
201 during *O. tsutsugamushi* infection that correlated with disease progression (Fig 2B). To validate
202 our findings mouse models, we measured scrub typhus patient sera via specific ELISA assays
203 and found a statistically significant increase in circulating Ang2 levels, which correlated with
204 their *O. tsutsugamushi*-specific antibody titers ($p < 0.05$ and $p < 0.01$, comparing IFA titers of
205 1:640 and 1:1280 with the control subjects, Fig 2C). These human data support our findings
206 obtained from mouse tissues, indicating the potential utility of serum Ang2 levels as a molecular
207 biomarker of scrub typhus severity.
208
209 IFA staining of the Ang1/2 receptor, Tie2, revealed clear Tie2 staining in mock infected controls,
210 however, positive Tie2 staining was nearly absent in some foci of D6 and D9 samples (Fig 3A).
211 To validate these findings, we used Western blot analyses of lung tissues and confirmed a
212 striking reduction of phosphorylated Tie2 (pTie2) and total Tie2 levels at both D6 and D9, as
213 compared with either the mock and D2 samples (Fig 3B), implying impairments at the
214 translational and functional levels. The qRT-PCR analyses further validated a statistically

215 significant decrease in *TIE2* mRNA levels in the lungs at D6 and D10 ($p < 0.01$, compared with
216 the mock controls, Fig 3C), implying impairment at the transcriptional level. These data, together
217 with our previous studies [32, 33], indicate that marked Ang2 production, accompanied with
218 severe impairment in the Tie2 functions, are pathogenic mechanisms of severe vascular damage
219 in *O. tsutsugamushi* infection.
220
221 **M1-like responses in the lungs of infected mice**
222 Having documented progressive endothelial damage and alterations in endothelium-specific
223 biomarkers following *O. tsutsugamushi* infection (Figs 1 and 2), we then examined the timing
224 and magnitude of leukocyte recruitment and activation. Although some reports described
225 leukocyte involvement in *O. tsutsugamushi*-infected mouse spleen and brain [34, 40], there are
226 no detailed studies of innate immune responses in infected lungs. Using immunofluorescent
227 staining, we found that $CD45^+$ leukocytes and $CD3^+$ T cells were accumulated around Ang2-
228 positive foci in the lungs at D6 and D10, and that CD45-Ang2 or CD3-Ang2 co-stained foci
229 were readily detectable at D10 (yellow, S2A Fig). Flow cytometric analyses revealed a 20-fold
230 increase in total numbers of $CD4^+$ T cells at D10, but a statistically significant decrease in
231 percentages of these cells at D6 and D10, respectively ($p < 0.0001$, compared with mock
232 controls, S2B Fig). In contrast, there was a 50-fold increase in total numbers and 2.3-fold
233 increase in percentages of $CD8^+$ T cells at D10 (S2C Fig). These findings were consistent with
234 the known importance of $CD8^+$ T cells during *O. tsutsugamushi* infection in mice [40, 41].
235
236 Monocytes and MΦs are particularly noteworthy leukocytes during *O. tsutsugamushi* infection,
237 as they can act as a target for bacterial replication and a propagator of the inflammatory response

238 [8, 14], possibly playing a role in *O. tsutsugamushi* dissemination from skin lesions [9, 42].
239 While *in vitro* infection predominantly drives human monocytes/MΦs to M1-like transcription
240 programs [9, 42], our current knowledge on *O. tsutsugamushi*-MΦ interactions in the lungs is
241 still limited. Using IFA staining, we observed co-localization of bacteria (green) with IBA-1$^+$
242 MΦs (red) in mouse lungs (S3A Fig). To define monocyte/MΦ responses, we applied reported
243 protocols and gating strategies for flow cytometric analysis of mouse lung monocyte/MΦ subsets
244 [43] (Fig 4A). Compared with the mock controls, D6 and D9 samples had 4- to 5-fold increases
245 in the frequency of CD64$^+$CD11b$^+$Ly6G$^-$ alveolar/interstitial monocytes/MΦs, as well as 6- and
246 14-fold increases in total cell numbers, respectively ($p < 0.01$ and $p < 0.001$, Fig 4B). Of note,
247 nearly all (~97%) pulmonary MΦs displayed an M1-like phenotype
248 (CD80$^+$CD64$^+$CD11b$^+$Ly6G$^-$, Fig 4C) at D9. In contrast, while the mock and D2 lung samples
249 contained ~3.2% of M2-like (CD206$^+$CD64$^+$CD11b$^+$Ly6G$^-$) cells, these cells were barely
250 detectable at D6 or D9 (Fig 4D). These data suggest extensive recruitment and/or activation of
251 M1-like cells, but marked loss and/or suppression of M2-like cells, during the progression of
252 disease. Likewise, lung qRT-PCR assays confirmed a significant up-regulation of M1 markers
253 (*IFNγ, FPR2, CD38*, and *NOS2*), but not M2 markers (*CD206*, *EGR2*), at D9 (Fig 5A and B).
254 While the *IL10* up-expression was previously reported by our lab and other groups [44], we also
255 detected an increased expression of *ARGINASE1* (Fig 5B), a marker known for M2 polarization
256 and the growth of other intracellular pathogens [45]. Together with data shown in Fig 4, we
257 concluded that at the onset of disease and beyond, *O. tsutsugamushi* infection preferentially
258 stimulated pro-inflammatory innate responses in M1-like monocytes/MΦs, which correlate with
259 the onset of vascular damage (Figs 1-3).
260

MΦ polarization in favor of *Orientia* replication *in vitro*

Because we had demonstrated differential monocyte/MΦ responses *in vivo*, we asked how MΦ polarization might influence intracellular growth of the bacteria. We generated bone marrow-derived MΦs from naïve C57BL/6 mice, polarized cells via pretreatment with LPS (100 ng/ml) or recombinant IL-4 (rIL-4, 10 ng/ml) for 24 h, infected cells with *O. tsutsugamushi* (MOI 5), and measured bacterial loads at different time points. Flow cytometry and gene profile analyses of primed but uninfected cells confirmed their corresponding polarization to either classically activated M1 or alternatively activated M2 phenotypes (S3B and C Fig), as documented by others [46]. At 48 h post-infection, IL-4-primed M2 cells contained significantly increased loads of bacteria (judged by the copy number of *Orientia* 47-kDa gene) than LPS-primed M1 cells ($p < 0.01$, Fig 6A). At 72 h post-infection, M2 cells contained 10-fold more bacteria than M1 cells (Fig 6A), with extensive accumulation of bacteria (green) within IBA-1-positive MΦs (red, Fig 6B).

Discussion

Despite being an important emerging infectious disease, detailed immunological studies of scrub typhus patient samples or *O. tsutsugamushi*-infected animal tissues during the course of disease are scarce. In this study, we focused on ECs and monocytes/MΦs in the lungs of lethally infected mice to examine the activation of these cellular subsets known to be important cellular targets of *O. tsutsugamushi in vivo*. Our findings revealed important parameters and cell-specific alterations associated with acute lung injury and pathogenesis. The endothelium in infected lungs presented progressive Tie2 malfunction, increased Ang2 and ICAM-1 expression and pro-inflammatory MΦs at the onset of disease and severe stages of infection. Since lung damage and

284 vascular malfunction are hallmarks of scrub typhus severity in patients [6], a better
285 understanding of pathogenesis associated with acute lung injury is important for disease control
286 and management.
287
288 The molecular characteristics of endothelial alterations during *O. tsutsugamushi* infection *in vivo*
289 have not been explored. The present study provided evidence for the mechanisms underlying
290 pulmonary injury and vascular dysfunction during *O. tsutsugamushi* infection. First, the timing
291 of ICAM-1 and VEGFR2 expression on the surface of lung-derived $CD31^{+}CD45^{-}$ ECs was
292 concurrent with the appearance of signs of vascular injury and decrease in cell junction proteins
293 (Fig 1 and S1 Fig). Since ICAM-1 promotes circulating immune cells to bind to the endothelium
294 and extravasate into inflamed tissues [47], increased ICAM-1 surface expression likely
295 contributed to immune cell influx into the infected mouse lungs (Fig 5, S2 Fig). Our observed
296 *ICAM1* and *IL-8/CXLC8* up-regulation in infected human EC cultures (S1C Fig) were consistent
297 with other reported studies of scrub typhus patients [48]. VEGFR2 is known to be the primary
298 receptor for vascular endothelial growth factor (VEGF) in the endothelium, and the
299 VEGF/VEGFR2 axis regulates microvascular permeability via interacting with VE-cadherin and
300 tight junction proteins [49, 50]. In our hands, we consistently detected a marked increase in
301 VEGFR2 on the surface of infected ECs, but a significant reduction of VE-cadherin (adhesion
302 junctions) in the lungs at D6 and D9. While it is unclear whether increased VEGFR2 expression
303 is directly linked to diminished VE-cadherin expression in infected lungs, our data suggest
304 compromised endothelial barrier integrity during severe *O. tsutsugamushi* infection in the lungs.
305

306 Second, a notable reduction of Tie2 proteins was concurrent with significant Ang2 production
307 and/or release at the severe stages of infection (Figs 2-3). To date, there are no reports for Tie2
308 expression levels in scrub typhus patients or animal models, although our group previously
309 showed increased *ANG2/ANG1* transcript ratios in *O. tsutsugamushi*-infected human EC cultures
310 and mouse tissues [32]. Our findings of significant and progressive reduction in Tie2 protein and
311 its mRNA levels, as well as functional pTie2 level, in the lungs of lethally infection mice are
312 important from basic research and clinical points of view. It is known that the Ang1/Tie2 axis is
313 essential for vascular remodeling and endothelial cell stabilization, as either knockout Ang1 or
314 Tie2 in mice is embryonic lethal [51, 52]. Given the critical function of Tie2 receptor in vascular
315 physiology and integrity, it will be important to further examine whether our observed reduction
316 in Ang1 and Tie2 is due to direct endothelial damage or signaling from nearby pericytes and
317 recruited immune cells. Research in these areas would be of great value, as angiopoietin- or
318 Tie2-targeted therapies have been evaluated as alternative treatment strategies for severe sepsis
319 [53, 54], severe dengue [55], and in cerebral malaria [38] infection models to restore endothelial
320 quiescence during infection. Our clinical observation that increased serum Ang2 in human scrub
321 typhus patients correlates with *O. tsutsugamushi*-specific antibody titers demonstrates the utility
322 of Ang2 as a pathogenic biomarker, and highlights the potential of use Ang2- or Tie2-targeted
323 therapies for severe scrub typhus, as in patients with severe sepsis [29, 30] and malaria [56].
324
325 Monocytes/MΦs play important roles in infection with *O. tsutsugamushi* and other closely
326 related *Rickettsia* species [19, 57]. Previous findings [19] are consistent with our observation of
327 an increased accumulation of $CD11b^{+}Ly6G^{-}$ MΦs/monocytes and the close association of $IBA\text{-}l^{+}$
328 phagocytes with *Orientia* in the lungs at D6 and D9. Yet, our findings of selective

329 recruitment/expansion of M1-skewed MΦs/monocytes, and the suppression of M2 cell
330 activation, in the infected mouse lungs were particularly novel and important. This is the first *in*
331 *vivo* evidence for M1-polarized MΦ responses in *O. tsutsugamushi*-infected mouse lungs, which
332 was consistent with previous *in vitro* and *ex vivo* studies for M1-skewed gene transcription
333 programs in *O. tsutsugamushi*-infected human monocytes and MΦs [21, 42]. At present, it is still
334 unclear whether the predominately M1 MΦ population we observed contributes to the killing of
335 *O. tsutsugamushi* and the damage of vascular tissues, as seen for protective versus pathogenic
336 roles in other lung infection models [58]. Given the reports that anti-Ang2 antibody treatment
337 during pulmonary bacterial infection can decrease MΦ recruitment and inflammation [26], and
338 that signaling via Tie2 on monocytes/MΦs can promote a proinflammatory profile [59], it will be
339 interesting to determine how Ang2/Ang1 signaling on both endothelial cells and MΦs promote
340 cellular recruitment and activation during *O. tsutsugamushi* infection.
341
342 Conditions that promote the killing or growth of *O. tsutsugamushi* remain unclear, in part due to
343 difficulties in bacterial cultivation, genetic modification, or visualization for studying the host-
344 bacterium interactions [60]. Currently, there are no available reports or data for the phenotype of
345 *Orientia*-carrying MΦ subsets or the roles of arginase-1 *in vivo*. Our *in vitro* comparative studies
346 revealed limited bacterial replication in LPS-primed M1-like MΦs (Fig 6), supporting a previous
347 report for the role of NOS2-mediated mechanisms in the control of *O. tsutsugamushi* Karp strain
348 [19]. Yet, our *in vitro* findings were contradictory to another reported study, in which NO-
349 enhanced the growth of *O. tsutsugamushi* Ikeda bacteria was observed in LPS-activated RAW
350 264.7 murine macrophages at days 6 to 8 post-infection [20]. While the use of different bacterial
351 strains, MΦ sources, and examination times may account for these discrepancies, our study calls

for careful examination of the intracellular niche for the replication of these obligate intracellular bacteria under different or physiological conditions. For bone marrow-derived MΦs, we found comparable bacterial loads in LPS- and IL-4-primed cells at 3 h, implying similar attachment and invasion of the bacteria under these two treatments. However, IL-4-primed M2 cells contained 10-fold more *O. tsutsugamushi* than LPS-primed M1 cells at 72 h. At present, our data did not exclude the possibility of bacterial growth in LPS-primed M1 cells after prolonged time *in vitro*, or in M1- vs. M2-like MΦs in mouse lungs or other organs. Given the recent report that specific MΦ responses, such as miR-155 and IL-10 production, correlate with prevention of cytokine storm in severe *O. tsutsugamushi* infection [61], it will be important to further examine whether the strong type-1 inflammatory responses *in vivo* [32] and M1-skewed responses (Fig 5) are responsible for marked decrease in M2 MΦs in the lungs. The use of transgenic mouse strains for tracking MΦ subsets would also help reveal whether *O. tsutsugamushi* bacteria preferentially replicate within M2 MΦs *in vitro* or contribute to the impairment of type 2 immune responses.

While the mouse model used here allows us to examine host-bacterium interactions and immune alterations, this model has some intrinsic limitations, as it bypasses bacterial dissemination from the local/skin sites. Nevertheless, this model has several advantages over self-limited infection models following the subcutaneous or intradermal inoculation of the bacteria via needles into inbred strains of mice [19, 62], for the examination of innate immune responses in visceral organs. Compared to a lethal infection initiated by feeding *O. tsutsugamushi*-infected mites on outbred mice, a technically challenging model with high variability [63], our model provides more consistent results and lethality, permitting the analysis of a given host molecule using gene-targeted knockouts on the C57BL/6 background. More importantly, our lethal model mimics

certain pathological aspects of severe scrub typhus observed in humans, uncovering tissue-specific immune alterations that have never been described previously. For example, our findings of elevated Ang2 proteins in *O. tsutsugamushi*-infected lungs and increased *ANG2* expression in multiple organs [32] are consistent with clinical studies of scrub typhus patients (Fig 2), which supports the potential for monitoring serum Ang2 levels as an indicator of disease severity and treatment outcome.

In summary, this study has revealed new insights into immune dysregulation and pathogenesis of severe scrub typhus. Through comprehensive analyses of *O. tsutsugamushi*-infected mouse lung tissues, we have provided the first evidence for the production of endothelial destabilizing factors and *in vivo* polarization of lung recruited MΦs. Our findings of polarized M1-like responses in the lungs at late stages of disease argue for immune-based restriction of bacterial replication as well as immunopathogenesis. While the molecular mechanisms underlying host-bacterium interaction and immune dysregulation remains unclear at this stage, it is conceivable that serum and tissue Ang2 levels would be a molecular biomarker for severe scrub typhus and a potential therapeutic target for treatment. A better understanding of infection- versus immune-mediated dysregulation will help design treatment strategies for severe scrub typhus cases.

Materials and Methods

Mouse infection and ethics statement

Female C57BL/6 mice were purchased from Envigo (Huntingdon, United Kingdom), maintained under specific pathogen-free conditions and used at 6-9 weeks of age, following protocols approved by the Institutional Animal Care and Use Committee (protocols # 9007082B and 1302003) at the University of Texas Medical Branch (UTMB) in Galveston, TX. All mouse infection studies were performed in the ABSL3 facility in the Galveston National Laboratory located at UTMB; all tissue processing and analysis procedures were performed in the BSL3 or BSL2 facilities. All procedures were approved by the Institutional Biosafety Committee, in accordance with Guidelines for Biosafety in Microbiological and Biomedical Laboratories. UTMB operates to comply with the USDA Animal Welfare Act (Public Law 89-544), the Health Research Extension Act of 1985 (Public Law 99-158), the Public Health Service Policy on Humane Care and Use of Laboratory Animals, and the NAS Guide for the Care and Use of Laboratory Animals (ISBN-13). UTMB is a registered Research Facility under the Animal Welfare Act, and has a current assurance on file with the Office of Laboratory Animal Welfare, in compliance with NIH Policy.

O. tsutsugamushi Karp strain was used herein; all infection studies were performed with the same bacterial stocks prepared from Vero cell infection, for which infectious organisms were quantified via a qPCR viability assay [35, 64]. Mice were inoculated intravenously (i.v.) with ~1.325×10^6 viable bacteria (a lethal dose, 200 µl) or PBS and monitored daily for weight

420 loss and signs of disease. In most cases, tissue samples (4-5 mice/group) were collected at 2, 6,
421 and 9 (or 10) days post-infection and inactivated for immediate or subsequent analyses.
422
423 Ethical approval for human samples used in this work was granted by the Institutional Review
424 Board of both Seoul National University Hospital (IRB NO 1603-136-751) and Chungnam
425 National University Hospital (IRB NO 2014-12-006). All patients and healthy volunteers
426 provided written informed consent prior to sample collection.
427
428 **Immunofluorescence microscopy and quantification**
429 Mouse lung tissues were processed for immunofluorescent staining, as in our previous report
430 [34]. Briefly, 6-μm frozen sections were blocked and incubated with the following rat or rabbit
431 anti-mouse antibodies (1:200, purchased from Abcam, Cambridge, MA, USA, unless specified):
432 anti-ICAM1, anti-Ang1, anti-Ang2 (R&D Systems/Biotechne, McKinley Place NE, Minnesota),
433 anti-Tie2, anti-VE-cadherin (adherence junctions), anti-occludin (epithelial tight junctions), anti-
434 IBA-1 (ionised calcium binding adapter molecule-1, a MΦ marker), anti-CD45 (BD Bioscience,
435 San Jose, CA, USA), or anti-Ang2 (R&D Systems). Staining endothelium in sections was done
436 with FITC-conjugated *Griffonia Simplicifolia* lectin I (1:100, GSL I-B_4 lectin, Vector Lab,
437 Burlingame, CA, USA). Bacteria was stained in various sections using rabbit anti-*O.*
438 *tsutsugamushi* Karp serum (1:500) [35]. Bound antibodies were visualized by using Alexa Fluor
439 488- or 555-conjugated, goat anti-rat or anti-rabbit IgG (H+L, 1:1,000-1:2,000, Life
440 Technologies, Grand Island, NY, USA). All sections were stained with DAPI (1:5,000, Sigma-
441 Aldrich, St. Louis, MO, USA). Infected sections stained with secondary Abs and DAPI only
442 served as negative controls to optimize staining conditions. For each section, at least 6 low- and

443 6 high-magnification fields of the lung sections were imaged on a Carl Zeiss Axio Observer
444 fluorescence microscope (Carl Zeiss Microscopy LLC, Thornwood, NY, USA) equipped with
445 ApoTome and Zen imaging software. Acquisition settings were identical among samples of
446 different experimental groups. Representative images at each time point are presented. To
447 measure fluorescent intensity of given markers, gray levels across the entire tissue image (low-
448 magnification, 4 independent images per group) were measured via ImageJ under the same
449 parameter setting. Data are presented at mean ± SEM of the group.
450
451 For *in vitro* studies, cells were seeded onto coverslips in 24-well plates (Falcon Corning,
452 Corning, NY, USA). At indicated times of infection, slides were washed, fixed with 4% PFA for
453 20 min, and permeabalized with Triton X-100 for 15 min. After blocking with 10% BSA/3%
454 goat serum for 1 h, cells were incubated with serum collected from *Orientia*-infected mice
455 (1:1,500) or rabbit anti-IBA-1 (1:250, Abcam) (1:50) at 4°C overnight and then with a secondary
456 Ab: goat anti-mouse Alexa Fluor 488 (Thermo Fisher Scientific, Waltham, MA, USA) or donkey
457 anti-rabbit Alexa Fluor 594 (Invitrogen/Thermo Fisher Scientific) and DAPI (1:1000, Thermo
458 Fisher Scientific). The cover slips were mounted on slides by using an Antifade Mountant
459 solution (Invitrogen/Thermo Fisher Scientific). Images were taken using an Olympus IX51
460 microscope (Olympus Corporation, Tokyo, Japan).
461
462 **Flow cytometry**
463 Equivalent portions of lung tissues were harvested from infected and control mice, minced, and
464 digested with 0.05% collagenase type IV (Gibco/Thermo Fisher Scientific) in Dulbecco's
465 Modified Eagle's Medium (DMEM, Sigma-Aldrich, St. Louis, MO) for 30 mins at 37°C.

Minced tissues were loaded into Medicons and homogenized using a BD Mediamachine System (BD Biosciences, Franklin Lakes, NJ). Lung single-cell suspensions were made by passing lung homogenates through 70-µm cell strainers. Spleen homogenates were made by passing tissue through a 70-µm strainer. Lymphocytes were enriched by using Lympholyte-M Cell Separation Media (Burlington, NC). Red blood cells were removed by using Red Cell Lysis Buffer (Sigma-Aldrich). Leukocytes were stained with the Fixable Viability Dye (eFluor 506) (eBioscience/Thermo Fisher Scientific, Walthalm, MA) for live/dead cell staining, blocked with FcγR blocker, and stained with fluorochrome-labeled antibodies (Abs). The following Abs purchased from Thermo Fisher Scientific and BioLegend (San Diego CA): PE-Cy7-anti-CD3ε (145-2C11), Pacific Blue-anti-CD4 (GK1.5), APC-Cy7-anti-CD8a (53-6.7), APC-anti-Ly6G (1A8-Ly6G), APC-anti-CD31 (390), PE-anti-VEGFR2 (Avas12a1), FITC-anti-ICAM-1 (YN1/1.7.4), Pacific Blue-anti-CD45 (30-F11), PE-anti-CD80 (16-10A1), BV421-anti-CD206 (CO68C2), FITC-anti-CD64 (X54-5/7.1), PerCP-Cy5.5-anti-CD11b (M1/70). Cells were fixed in 2% paraformaldehyde overnight at 4°C before cell analysis. Data were collected by a BD LSRFortessa (Becton Dickinson, San Jose, CA) and analyzed using FlowJo software version 8.86 (Tree Star, Ashland, OR). As previously reported for mouse lung tissues [65] $CD45^{+}CD31^{-}$ and $CD45^{-}CD31^{+}$ cells were considered hematopoietic cells and endothelial cells by flow cytometry, respectively.

Western blot

Protein from lung tissues was extracted with a RIPA lysis buffer (Cell Signaling Technology, Danvers, MA) and quantified with BCA Protein Assay kit (Thermo Fisher Scientific). Protein samples (40 µg/lane) were loaded onto 4-20% SDS-PAGE gels (Bio-Rad Laboritories, Hercules,

CA, USA) and transferred onto nitrocellulose membranes (Bio-Rad Laboratories). After blocking non-specific binding sites, membranes were respectively incubated with rabbit Abs specific to mouse Tie2 (1:500, Abcam), phospho-Tie2 (1:400, R&D System, USA), and β-actin (1:15000, Novus Biologicals, USA), and an anti-rabbit secondary antibody (SouthernBiotech, Birmingham, AL, USA). After treatment with the Maximum Sensitivity Substrate (Thermo Fisher Scientific) for 1 min, the light signals were captured by Luminescent Image Analyzer (ImageQuant LAS 4000, GE Healthcare Bio-Sciences AB, Sweden). Protein bands were quantified by using image analysis software (ImageJ). Three independent experiments were performed.

Infection of mouse bone marrow-derived MΦs

Bone marrow cells were collected from mouse femur and tibia and treated with a red cell lysis buffer (Sigma). For MΦ generation, bone marrow cells were grown in DMEM (Gibco) with 10% FBS, penicillin/streptomycin antibiotics, and 40 ng/ml M-CSF (BioLegend) and incubated at 37°C. Media was changed at day 3, and cells were collected at day 7 and seeded onto 6- or 24-well plates for overnight. MΦs were treated with either 100 ng/ml LPS (for M1 polarization) or 10 ng/ml mouse rIL-4 (for M2 polarization, Peprotech, Rocky Hill, NJ) for 24 h. Cells were then infected with *O. tsutsugamushi* (5 MOI) and centrifuged at 2,000 RPM for 5 min to synchronize infection of the cells.

510 **Quantitative PCR and reverse transcriptase PCR (qPCR and qRT-PCR)**

511 To determine bacterial loads, bone marrow-derived MΦs were collected at 3, 24, 48, and 72 hpi
512 by using a DNeasy kit (Qiagen) and used for qPCR assays, as previously described [32].
513 Bacterial loads were normalized to total nanogram (ng) of DNA per µL for the same sample, and
514 data are expressed as the gene copy number of 47-kDa protein per picogram (pg) of DNA. The
515 copy number for the 47-kDa gene was determined by known concentrations of a control plasmid
516 containing single-copy insert of the gene. Gene copy numbers were determined via serial dilution
517 (10-fold) of the control plasmid.

518

519 To measure host gene expression, mouse tissues or *in vitro*-infected cells were respectively
520 collected in RNA*Later* (Ambion, Austin, TX) or Trizol solution at 4°C overnight to inactivate
521 infectious bacteria and stored at -80°C for subsequent analyses. Total RNA was extracted by
522 using RNeasy mini kits (Qiagen) and digested with RNase-free DNase (Qiagen); cDNA was
523 synthesized with the iScript cDNA synthesis kit (Bio-Rad Laboratories, Hercules, CA). The
524 quantitative RT-PCR (qRT-PCR) assays were performed with iTaq SYBR Green Supermix and a
525 CFX96 Touch Real-Time PCR Detection System (Bio-Rad). PCR assays were denatured for 3
526 min at 95°C, followed by 40 cycles of 10s at 95°C and 30s at 60°C. Melt-curve analysis was also
527 used to check the specificity of the amplification reaction. Relative abundance of transcripts was
528 calculated by using the $2^{-\Delta\Delta CT}$ method and compared to housekeeping genes glyceraldehyde-3-
529 phosphate dehydrogenase (GAPDH) or β-actin. Primers used in these analyses are listed in Table
530 S1.

531

532 **Human umbilical vein endothelial cell (HUVEC) infection**

HUVECs (Cell Application, San Diego, CA) were maintained in complete Prigrow I medium supplemented with 3% heat-inactivated FBS (Applied Biological Materials, Vancouver, Canada) in 5% CO_2 at 37°C. All *in vitro* experiments were performed between cell passages 5 and 7, as described previously [33, 66]. For infection, HUVECs were cultivated in Prigrow I medium with 10% FBS and seeded onto 6-well plates (Corning Inc., Corning, NY). Confluent monolayers were infected with *Orientia* (3 and 10 MOI) for 24 h and compared with uninfected controls.

Human serum collection and measurement of Ang2 by ELISA

Human serum samples were collected from healthy volunteers (n = 8) and scrub typhus patients (n = 32) after obtaining informed consent at the Chungnam National University Hospital in Daejeon, South Korea. Scrub typhus diagnosis was confirmed based on clinical symptoms and a positive serology: a 4-fold or greater rise in the titer of paired plasma or single cut-off titer of an IgM antibody ≥ 1:160 by an indirect immunofluorescence antibody assay (IFA) against *O. tsutsugamushi* antigens or passive hemagglutination assay (PHA) during hospital admission. Healthy volunteers had never been previously diagnosed with scrub typhus, and their sera were negative when examined by IFA. Patient plasma samples were classified into four groups based on their IFA titers. Ang2 concentration was determined by using a commercial ELISA kit (Abcam), according to manufacturer's instructions.

Human antibody titer measured by IFA

L929 cells infected with three strains of *O. tsutsugamushi* (Boryong, Karp, and Gilliam strains) were harvested, mixed in equal amounts, and used as antigens to measure total IgG titers against *O. tsutsugamushi* via IFA. Briefly, infected L929 cells were harvested, washed with PBS, seeded

556 onto Teflon-coated spot slides, and fixed with cold acetone for 10 min. The slides were stored at
557 -70°C until use. Two-fold serially diluted (1:40 to 1:1280 in PBS) patient sera was added to the
558 antigen-coated spot on the slide and incubated for 30 min in a wet chamber at room temperature.
559 An Alexa Fluor 488-conjugated goat anti-human IgG (diluted 1:1000 in PBS, Molecular Probes,
560 Waltham, MA, USA) was used as the secondary antibody. The stained slides were examined
561 under an Olympus FV1000 laser scanning confocal microscope (Olympus, Tokyo, Japan). The
562 endpoint titer of IFA was defined as the highest titer showing a fluorescence signal above the
563 background.
564
565 **Statistical analysis**
566 Data were presented as mean ± standard errors of the mean (SEM). Differences between
567 individual treatment and control groups were determined by using Student's t test, utilizing
568 Welch's correction when appropriate. One-way ANOVA was used for multiple group
569 comparisons with a Tukey's Post Hoc for comparisons between groups. Statistically significant
570 values are referred to as *, $p<0.05$; **, $p<0.01$; ***, $p<0.001$; and ****, $p<0.0001$.
571

572 ## Acknowledgements

573 The authors thank Dr. David Walker for generously providing BSL-3 laboratory equipment and
574 space for conducting experiments, Nicole Mendell for continued training and technical help in
575 many aspects of this study, Dr. Juan Olano and the UTMB Immunology Joint Lab Group for
576 providing helpful suggestions, and Dr. Sherry Haller for manuscript editing assistance.
577
578

References

1. Paris DH, Shelite TR, Day NP, Walker DH. Unresolved problems related to scrub typhus: a seriously neglected life-threatening disease. Am J Trop Med Hyg. 2013;89(2):301-7. doi: 10.4269/ajtmh.13-0064. PubMed PMID: 23926142; PubMed Central PMCID: PMCPMC3741252.

2. Kim G, Ha NY, Min CK, Kim HI, Yen NT, Lee KH, et al. Diversification of Orientia tsutsugamushi genotypes by intragenic recombination and their potential expansion in endemic areas. PLoS Negl Trop Dis. 2017;11(3):e0005408. Epub 2017/03/01. doi: 10.1371/journal.pntd.0005408. PubMed PMID: 28248956; PubMed Central PMCID: PMCPMC5348041.

3. Brown GW, Robinson DM, Huxsoll DL, Ng TS, Lim KJ. Scrub typhus: a common cause of illness in indigenous populations. Trans R Soc Trop Med Hyg. 1976;70(5-6):444-8. PubMed PMID: 402722.

4. Phongmany S, Rolain JM, Phetsouvanh R, Blacksell SD, Soukkhaseum V, Rasachack B, et al. Rickettsial infections and fever, Vientiane, Laos. Emerg Infect Dis. 2006;12(2):256-62. doi: 10.3201/eid1202.050900. PubMed PMID: 16494751; PubMed Central PMCID: PMCPMC3373100.

5. Varghese GM, Janardhanan J, Trowbridge P, Peter JV, Prakash JA, Sathyendra S, et al. Scrub typhus in South India: clinical and laboratory manifestations, genetic variability, and outcome. Int J Infect Dis. 2013;17(11):e981-7. Epub 2013/07/26. doi: 10.1016/j.ijid.2013.05.017. PubMed PMID: 23891643.

6. Hsu YH, Chen HI. Pulmonary pathology in patients associated with scrub typhus. Pathology. 2008;40(3):268-71. doi: 10.1080/00313020801911488. PubMed PMID: 18428046.

602 7. Wang CC, Liu SF, Liu JW, Chung YH, Su MC, Lin MC. Acute respiratory distress
603 syndrome in scrub typhus. Am J Trop Med Hyg. 2007;76(6):1148-52. PubMed PMID:
604 17556627.
605 8. Moron CG, Popov VL, Feng HM, Wear D, Walker DH. Identification of the target cells
606 of Orientia tsutsugamushi in human cases of scrub typhus. Mod Pathol. 2001;14(8):752-9. doi:
607 10.1038/modpathol.3880385. PubMed PMID: 11504834.
608 9. Paris DH, Phetsouvanh R, Tanganuchitcharnchai A, Jones M, Jenjaroen K, Vongsouvath
609 M, et al. Orientia tsutsugamushi in human scrub typhus eschars shows tropism for dendritic cells
610 and monocytes rather than endothelium. PLoS Negl Trop Dis. 2012;6(1):e1466. Epub
611 2012/01/10. doi: 10.1371/journal.pntd.0001466. PubMed PMID: 22253938; PubMed Central
612 PMCID: PMCPMC3254662.
613 10. Koo JE, Hong HJ, Dearth A, Kobayashi KS, Koh YS. Intracellular invasion of Orientia
614 tsutsugamushi activates inflammasome in asc-dependent manner. PLoS One. 2012;7(6):e39042.
615 Epub 2012/06/18. doi: 10.1371/journal.pone.0039042. PubMed PMID: 22723924; PubMed
616 Central PMCID: PMCPMC3377614.
617 11. Chu H, Lee JH, Han SH, Kim SY, Cho NH, Kim IS, et al. Exploitation of the endocytic
618 pathway by Orientia tsutsugamushi in nonprofessional phagocytes. Infect Immun.
619 2006;74(7):4246-53. doi: 10.1128/IAI.01620-05. PubMed PMID: 16790799; PubMed Central
620 PMCID: PMCPMC1489698.
621 12. Cho NH, Seong SY, Huh MS, Kim NH, Choi MS, Kim IS. Induction of the gene
622 encoding macrophage chemoattractant protein 1 by Orientia tsutsugamushi in human endothelial
623 cells involves activation of transcription factor activator protein 1. Infect Immun.
624 2002;70(9):4841-50. PubMed PMID: 12183528; PubMed Central PMCID: PMCPMC128290.

13. Cho KA, Jun YH, Suh JW, Kang JS, Choi HJ, Woo SY. Orientia tsutsugamushi induced endothelial cell activation via the NOD1-IL-32 pathway. Microb Pathog. 2010;49(3):95-104. Epub 2010/05/12. doi: 10.1016/j.micpath.2010.05.001. PubMed PMID: 20470879.

14. Cho NH, Seong SY, Huh MS, Han TH, Koh YS, Choi MS, et al. Expression of chemokine genes in murine macrophages infected with Orientia tsutsugamushi. Infect Immun. 2000;68(2):594-602. PubMed PMID: 10639422; PubMed Central PMCID: PMCPMC97181.

15. Kim MK, Kee SH, Cho KA, Chung MH, Lim BU, Chang WH, et al. Apoptosis of endothelial cell line ECV304 persistently infected with Orientia tsutsugamushi. Microbiol Immunol. 1999;43(8):751-7. PubMed PMID: 10524792.

16. Soong L. Dysregulated Th1 Immune and Vascular Responses in Scrub Typhus Pathogenesis. J Immunol. 2018;200(4):1233-40. doi: 10.4049/jimmunol.1701219. PubMed PMID: 29431689; PubMed Central PMCID: PMCPMC5812358.

17. Sunyakumthorn P, Paris DH, Chan TC, Jones M, Luce-Fedrow A, Chattopadhyay S, et al. An intradermal inoculation model of scrub typhus in Swiss CD-1 mice demonstrates more rapid dissemination of virulent strains of Orientia tsutsugamushi. PLoS One. 2013;8(1):e54570. Epub 2013/01/16. doi: 10.1371/journal.pone.0054570. PubMed PMID: 23342173; PubMed Central PMCID: PMCPMC3546997.

18. Otterdal K, Janardhanan J, Astrup E, Ueland T, Prakash JA, Lekva T, et al. Increased endothelial and macrophage markers are associated with disease severity and mortality in scrub typhus. J Infect. 2014;69(5):462-9. Epub 2014/07/01. doi: 10.1016/j.jinf.2014.06.018. PubMed PMID: 24995849.

19. Keller CA, Hauptmann M, Kolbaum J, Gharaibeh M, Neumann M, Glatzel M, et al. Dissemination of Orientia tsutsugamushi and inflammatory responses in a murine model of scrub

typhus. PLoS Negl Trop Dis. 2014;8(8):e3064. Epub 2014/08/14. doi: 10.1371/journal.pntd.0003064. PubMed PMID: 25122501; PubMed Central PMCID: PMCPMC4133189.

20. Ogawa M, Satoh M, Kataoka M, Ando S, Saijo M. Nitric oxide enhanced the growth of an obligated intracellular bacterium Orientia tsutsugamushi in murine macrophages. Microb Pathog. 2017;107:335-40. Epub 2017/04/12. doi: 10.1016/j.micpath.2017.04.012. PubMed PMID: 28412201.

21. Tantibhedhyangkul W, Ben Amara A, Textoris J, Gorvel L, Ghigo E, Capo C, et al. Orientia tsutsugamushi, the causative agent of scrub typhus, induces an inflammatory program in human macrophages. Microb Pathog. 2013;55:55-63. Epub 2012/10/23. doi: 10.1016/j.micpath.2012.10.001. PubMed PMID: 23088884.

22. Grommes J, Soehnlein O. Contribution of neutrophils to acute lung injury. Mol Med. 2011;17(3-4):293-307. doi: 10.2119/molmed.2010.00138. PubMed PMID: 21046059; PubMed Central PMCID: PMCPMC3060975.

23. Milam KE, Parikh SM. The angiopoietin-Tie2 signaling axis in the vascular leakage of systemic inflammation. Tissue Barriers. 2015;3(1-2):e957508. Epub 2015/04/03. doi: 10.4161/21688362.2014.957508. PubMed PMID: 25838975; PubMed Central PMCID: PMCPMC4372013.

24. Thurston G, Rudge JS, Ioffe E, Zhou H, Ross L, Croll SD, et al. Angiopoietin-1 protects the adult vasculature against plasma leakage. Nat Med. 2000;6(4):460-3. doi: 10.1038/74725. PubMed PMID: 10742156.

25. Fiedler U, Scharpfenecker M, Koidl S, Hegen A, Grunow V, Schmidt JM, et al. The Tie-2 ligand angiopoietin-2 is stored in and rapidly released upon stimulation from endothelial cell

671 Weibel-Palade bodies. Blood. 2004;103(11):4150-6. Epub 2004/02/19. doi: 10.1182/blood-2003-
672 10-3685. PubMed PMID: 14976056.
673 26. Tabruyn SP, Colton K, Morisada T, Fuxe J, Wiegand SJ, Thurston G, et al. Angiopoietin-
674 2-driven vascular remodeling in airway inflammation. Am J Pathol. 2010;177(6):3233-43. Epub
675 2010/10/15. doi: 10.2353/ajpath.2010.100059. PubMed PMID: 20952594; PubMed Central
676 PMCID: PMCPMC2993300.
677 27. Maisonpierre PC, Suri C, Jones PF, Bartunkova S, Wiegand SJ, Radziejewski C, et al.
678 Angiopoietin-2, a natural antagonist for Tie2 that disrupts in vivo angiogenesis. Science.
679 1997;277(5322):55-60. PubMed PMID: 9204896.
680 28. Fiedler U, Reiss Y, Scharpfenecker M, Grunow V, Koidl S, Thurston G, et al.
681 Angiopoietin-2 sensitizes endothelial cells to TNF-alpha and has a crucial role in the induction of
682 inflammation. Nat Med. 2006;12(2):235-9. Epub 2006/02/05. doi: 10.1038/nm1351. PubMed
683 PMID: 16462802.
684 29. Parikh SM, Mammoto T, Schultz A, Yuan HT, Christiani D, Karumanchi SA, et al.
685 Excess circulating angiopoietin-2 may contribute to pulmonary vascular leak in sepsis in
686 humans. PLoS Med. 2006;3(3):e46. doi: 10.1371/journal.pmed.0030046. PubMed PMID:
687 16417407; PubMed Central PMCID: PMCPMC1334221.
688 30. Orfanos SE, Kotanidou A, Glynos C, Athanasiou C, Tsigkos S, Dimopoulou I, et al.
689 Angiopoietin-2 is increased in severe sepsis: correlation with inflammatory mediators. Crit Care
690 Med. 2007;35(1):199-206. doi: 10.1097/01.CCM.0000251640.77679.D7. PubMed PMID:
691 17110873.
692 31. Petersen JE, Mkumbaye SI, Vaaben AV, Manjurano A, Lyimo E, Kavishe RA, et al.
693 Plasma Ang2 and ADAM17 levels are elevated during clinical malaria; Ang2 level correlates

694 with severity and expression of EPCR-binding PfEMP1. Sci Rep. 2016;6:35950. Epub
695 2016/10/27. doi: 10.1038/srep35950. PubMed PMID: 27784899; PubMed Central PMCID:
696 PMCPMC5082358.
697 32. Soong L, Wang H, Shelite TR, Liang Y, Mendell NL, Sun J, et al. Strong type 1, but
698 impaired type 2, immune responses contribute to Orientia tsutsugamushi-induced pathology in
699 mice. PLoS Negl Trop Dis. 2014;8(9):e3191. doi: 10.1371/journal.pntd.0003191. PubMed
700 PMID: 25254971; PubMed Central PMCID: PMCPMC4177881.
701 33. Shelite TR, Liang Y, Wang H, Mendell NL, Trent BJ, Sun J, et al. IL-33-Dependent
702 Endothelial Activation Contributes to Apoptosis and Renal Injury in Orientia tsutsugamushi-
703 Infected Mice. PLoS Negl Trop Dis. 2016;10(3):e0004467. doi: 10.1371/journal.pntd.0004467.
704 PubMed PMID: 26943125; PubMed Central PMCID: PMCPMC4778942.
705 34. Soong L, Shelite TR, Xing Y, Kodakandla H, Liang Y, Trent BJ, et al. Type 1-skewed
706 neuroinflammation and vascular damage associated with Orientia tsutsugamushi infection in
707 mice. PLoS Negl Trop Dis. 2017;11(7):e0005765. Epub 2017/07/24. doi:
708 10.1371/journal.pntd.0005765. PubMed PMID: 28742087; PubMed Central PMCID:
709 PMCPMC5542690.
710 35. Shelite TR, Saito TB, Mendell NL, Gong B, Xu G, Soong L, et al. Hematogenously
711 disseminated Orientia tsutsugamushi-infected murine model of scrub typhus [corrected]. PLoS
712 Negl Trop Dis. 2014;8(7):e2966. doi: 10.1371/journal.pntd.0002966. PubMed PMID: 25010338;
713 PubMed Central PMCID: PMCPMC4091938.
714 36. Gonzales JN, Lucas R, Verin AD. The Acute Respiratory Distress Syndrome:
715 Mechanisms and Perspective Therapeutic Approaches. Austin J Vasc Med. 2015;2(1). PubMed
716 PMID: 26973981; PubMed Central PMCID: PMCPMC4786180.

717 37. Heitrich M, García DM, Stoyanoff TR, Rodríguez JP, Todaro JS, Aguirre MV.
718 Erythropoietin attenuates renal and pulmonary injury in polymicrobial induced-sepsis through
719 EPO-R, VEGF and VEGF-R2 modulation. Biomed Pharmacother. 2016;82:606-13. Epub
720 2016/06/11. doi: 10.1016/j.biopha.2016.05.045. PubMed PMID: 27470403.
721 38. Ghosh CC, David S, Zhang R, Berghelli A, Milam K, Higgins SJ, et al. Gene control of
722 tyrosine kinase TIE2 and vascular manifestations of infections. Proc Natl Acad Sci U S A.
723 2016;113(9):2472-7. Epub 2016/02/16. doi: 10.1073/pnas.1519467113. PubMed PMID:
724 26884170; PubMed Central PMCID: PMCPMC4780619.
725 39. Parikh SM. The Angiopoietin-Tie2 Signaling Axis in Systemic Inflammation. J Am Soc
726 Nephrol. 2017;28(7):1973-82. Epub 2017/05/02. doi: 10.1681/ASN.2017010069. PubMed
727 PMID: 28465380; PubMed Central PMCID: PMCPMC5491297.
728 40. Xu G, Mendell NL, Liang Y, Shelite TR, Goez-Rivillas Y, Soong L, et al. Correction:
729 CD8+ T cells provide immune protection against murine disseminated endotheliotropic Orientia
730 tsutsugamushi infection. PLoS Negl Trop Dis. 2017;11(12):e0006127. Epub 2017/12/06. doi:
731 10.1371/journal.pntd.0006127. PubMed PMID: 29211737; PubMed Central PMCID:
732 PMCPMC5718426.
733 41. Hauptmann M, Kolbaum J, Lilla S, Wozniak D, Gharaibeh M, Fleischer B, et al.
734 Protective and Pathogenic Roles of CD8+ T Lymphocytes in Murine Orientia tsutsugamushi
735 Infection. PLoS Negl Trop Dis. 2016;10(9):e0004991. Epub 2016/09/08. doi:
736 10.1371/journal.pntd.0004991. PubMed PMID: 27606708; PubMed Central PMCID:
737 PMCPMC5015871.
738 42. Tantibhedhyangkul W, Prachason T, Waywa D, El Filali A, Ghigo E, Thongnoppakhun
739 W, et al. Orientia tsutsugamushi stimulates an original gene expression program in monocytes:

740 relationship with gene expression in patients with scrub typhus. PLoS Negl Trop Dis.
741 2011;5(5):e1028. Epub 2011/05/17. doi: 10.1371/journal.pntd.0001028. PubMed PMID:
742 21610853; PubMed Central PMCID: PMCPMC3096591.
743 43. Misharin AV, Morales-Nebreda L, Mutlu GM, Budinger GR, Perlman H. Flow
744 cytometric analysis of macrophages and dendritic cell subsets in the mouse lung. Am J Respir
745 Cell Mol Biol. 2013;49(4):503-10. doi: 10.1165/rcmb.2013-0086MA. PubMed PMID:
746 23672262; PubMed Central PMCID: PMCPMC3824047.
747 44. Min CK, Kim HI, Ha NY, Kim Y, Kwon EK, Yen NTH, et al. A Type I Interferon and
748 IL-10 Induced by. Front Immunol. 2018;9:2022. Epub 2018/09/04. doi:
749 10.3389/fimmu.2018.02022. PubMed PMID: 30233599; PubMed Central PMCID:
750 PMCPMC6131522.
751 45. Buchacher T, Ohradanova-Repic A, Stockinger H, Fischer MB, Weber V. M2
752 Polarization of Human Macrophages Favors Survival of the Intracellular Pathogen Chlamydia
753 pneumoniae. PLoS One. 2015;10(11):e0143593. Epub 2015/11/25. doi:
754 10.1371/journal.pone.0143593. PubMed PMID: 26606059; PubMed Central PMCID:
755 PMCPMC4659546.
756 46. Ying W, Cheruku PS, Bazer FW, Safe SH, Zhou B. Investigation of macrophage
757 polarization using bone marrow derived macrophages. J Vis Exp. 2013;(76). Epub 2013/06/23.
758 doi: 10.3791/50323. PubMed PMID: 23851980; PubMed Central PMCID: PMCPMC3728835.
759 47. Rothlein R, Dustin ML, Marlin SD, Springer TA. A human intercellular adhesion
760 molecule (ICAM-1) distinct from LFA-1. J Immunol. 1986;137(4):1270-4. PubMed PMID:
761 3525675.

762 48. Paris DH, Jenjaroen K, Blacksell SD, Phetsouvanh R, Wuthiekanun V, Newton PN, et al.
763 Differential patterns of endothelial and leucocyte activation in 'typhus-like' illnesses in Laos and
764 Thailand. Clin Exp Immunol. 2008;153(1):63-7. Epub 2008/05/23. doi: 10.1111/j.1365-
765 2249.2008.03673.x. PubMed PMID: 18505434; PubMed Central PMCID: PMCPMC2432098.
766 49. Dejana E, Orsenigo F, Lampugnani MG. The role of adherens junctions and VE-cadherin
767 in the control of vascular permeability. J Cell Sci. 2008;121(Pt 13):2115-22. doi:
768 10.1242/jcs.017897. PubMed PMID: 18565824.
769 50. Coon BG, Baeyens N, Han J, Budatha M, Ross TD, Fang JS, et al. Intramembrane
770 binding of VE-cadherin to VEGFR2 and VEGFR3 assembles the endothelial mechanosensory
771 complex. J Cell Biol. 2015;208(7):975-86. Epub 2015/03/23. doi: 10.1083/jcb.201408103.
772 PubMed PMID: 25800053; PubMed Central PMCID: PMCPMC4384728.
773 51. Dumont DJ, Gradwohl G, Fong GH, Puri MC, Gertsenstein M, Auerbach A, et al.
774 Dominant-negative and targeted null mutations in the endothelial receptor tyrosine kinase, tek,
775 reveal a critical role in vasculogenesis of the embryo. Genes Dev. 1994;8(16):1897-909. doi:
776 10.1101/gad.8.16.1897. PubMed PMID: 7958865.
777 52. Jeansson M, Gawlik A, Anderson G, Li C, Kerjaschki D, Henkelman M, et al.
778 Angiopoietin-1 is essential in mouse vasculature during development and in response to injury. J
779 Clin Invest. 2011;121(6):2278-89. doi: 10.1172/JCI46322. PubMed PMID: 21606590; PubMed
780 Central PMCID: PMCPMC3104773.
781 53. David S, Park JK, Meurs M, Zijlstra JG, Koenecke C, Schrimpf C, et al. Acute
782 administration of recombinant Angiopoietin-1 ameliorates multiple-organ dysfunction syndrome
783 and improves survival in murine sepsis. Cytokine. 2011;55(2):251-9. Epub 2011/04/30. doi:
784 10.1016/j.cyto.2011.04.005. PubMed PMID: 21531574.

785 54. Stiehl T, Thamm K, Kaufmann J, Schaeper U, Kirsch T, Haller H, et al. Lung-targeted
786 RNA interference against angiopoietin-2 ameliorates multiple organ dysfunction and death in
787 sepsis. Crit Care Med. 2014;42(10):e654-62. doi: 10.1097/CCM.0000000000000524. PubMed
788 PMID: 25083983.
789 55. Phanthanawiboon S, Limkittikul K, Sakai Y, Takakura N, Saijo M, Kurosu T. Acute
790 Systemic Infection with Dengue Virus Leads to Vascular Leakage and Death through Tumor
791 Necrosis Factor-α and Tie2/Angiopoietin Signaling in Mice Lacking Type I and II Interferon
792 Receptors. PLoS One. 2016;11(2):e0148564. Epub 2016/02/04. doi:
793 10.1371/journal.pone.0148564. PubMed PMID: 26844767; PubMed Central PMCID:
794 PMCPMC4742241.
795 56. Higgins SJ, Purcell LA, Silver KL, Tran V, Crowley V, Hawkes M, et al. Dysregulation
796 of angiopoietin-1 plays a mechanistic role in the pathogenesis of cerebral malaria. Sci Transl
797 Med. 2016;8(358):358ra128. doi: 10.1126/scitranslmed.aaf6812. PubMed PMID: 27683553.
798 57. Curto P, Simões I, Riley SP, Martinez JJ. Differences in Intracellular Fate of Two
799 Spotted Fever Group Rickettsia in Macrophage-Like Cells. Front Cell Infect Microbiol.
800 2016;6:80. Epub 2016/07/29. doi: 10.3389/fcimb.2016.00080. PubMed PMID: 27525249;
801 PubMed Central PMCID: PMCPMC4965480.
802 58. Aggarwal NR, King LS, D'Alessio FR. Diverse macrophage populations mediate acute
803 lung inflammation and resolution. Am J Physiol Lung Cell Mol Physiol. 2014;306(8):L709-25.
804 Epub 2014/02/07. doi: 10.1152/ajplung.00341.2013. PubMed PMID: 24508730; PubMed
805 Central PMCID: PMCPMC3989724.
806 59. Garcia S, Krausz S, Ambarus CA, Fernandez BM, Hartkamp LM, van Es IE, et al. Tie2
807 signaling cooperates with TNF to promote the pro-inflammatory activation of human

macrophages independently of macrophage functional phenotype. PLoS One. 2014;9(1):e82088. doi: 10.1371/journal.pone.0082088. PubMed PMID: 24404127; PubMed Central PMCID: PMCPMC3880273.

60. Díaz FE, Abarca K, Kalergis AM. An Update on Host-Pathogen Interplay and Modulation of Immune Responses during Orientia tsutsugamushi Infection. Clin Microbiol Rev. 2018;31(2). Epub 2018/01/31. doi: 10.1128/CMR.00076-17. PubMed PMID: 29386235; PubMed Central PMCID: PMCPMC5967693.

61. Tsai MH, Chang CH, Tsai RK, Hong YR, Chuang TH, Fan KT, et al. Cross-Regulation of Proinflammatory Cytokines by Interleukin-10 and miR-155 in Orientia tsutsugamushi-Infected Human Macrophages Prevents Cytokine Storm. J Invest Dermatol. 2016;136(7):1398-407. Epub 2016/02/24. doi: 10.1016/j.jid.2015.11.034. PubMed PMID: 26921773.

62. Soong L, Mendell NL, Olano JP, Rockx-Brouwer D, Xu G, Goez-Rivillas Y, et al. An Intradermal Inoculation Mouse Model for Immunological Investigations of Acute Scrub Typhus and Persistent Infection. PLoS Negl Trop Dis. 2016;10(8):e0004884. Epub 2016/08/01. doi: 10.1371/journal.pntd.0004884. PubMed PMID: 27479584; PubMed Central PMCID: PMCPMC4968841.

63. Lurchachaiwong W, Monkanna T, Leepitakrat S, Ponlawat A, Sattabongkot J, Schuster AL, et al. Variable clinical responses of a scrub typhus outbred mouse model to feeding by Orientia tsutsugamushi infected mites. Exp Appl Acarol. 2012;58(1):23-34. Epub 2012/04/24. doi: 10.1007/s10493-012-9563-8. PubMed PMID: 22527840.

64. Mendell NL, Bouyer DH, Walker DH. Murine models of scrub typhus associated with host control of Orientia tsutsugamushi infection. PLoS Negl Trop Dis. 2017;11(3):e0005453.

Epub 2017/03/10. doi: 10.1371/journal.pntd.0005453. PubMed PMID: 28282373; PubMed Central PMCID: PMCPMC5362142.

65. Singer BD, Mock JR, D'Alessio FR, Aggarwal NR, Mandke P, Johnston L, et al. Flow-cytometric method for simultaneous analysis of mouse lung epithelial, endothelial, and hematopoietic lineage cells. Am J Physiol Lung Cell Mol Physiol. 2016;310(9):L796-801. Epub 2016/03/04. doi: 10.1152/ajplung.00334.2015. PubMed PMID: 26944088; PubMed Central PMCID: PMCPMC4867353.

66. Gong B, Shelite T, Mei FC, Ha T, Hu Y, Xu G, et al. Exchange protein directly activated by cAMP plays a critical role in bacterial invasion during fatal rickettsioses. Proc Natl Acad Sci U S A. 2013;110(48):19615-20. Epub 2013/11/11. doi: 10.1073/pnas.1314400110. PubMed PMID: 24218580; PubMed Central PMCID: PMCPMC3845138.

Figure Legends

Fig 1. Endothelial cell (EC) activation and vascular damage in the lungs of *O. tsutsugamushi*-infected mice and in infected HUVECs *in vitro*. Female C57BL/6J mice were inoculated with 1.325 x 10^6 of *O. tsutsugamushi* Karp strain (4-5 mice/group) or PBS (3-4 mice/group). At days 2, 6, or 9 post-infection, equivalent lung portions were collected for analyses. (A) Frozen lung sections were co-stained for *Orientia* bacteria (red), ICAM-1 (green), and DAPI (blue, top row, scale bar = 50 μm) with close-up views of the boxed areas in the bottom row (bar = 20 μm). (B) Lung sections were co-stained for VE-cadherin (adherens junctions, red), FITC-labeled I-B_4 lectins (green), and DAPI (blue, top row, bars = 50 μm). Close-up views of the boxed areas located the bottom row (bar = 20 μm). (C) Quantification of fluorescent ICAM-1 and VE-Cadherin staining (four images per time point). (D) Lung-derived cells were analyzed via flow cytometry for the percentage of ICAM-1^+ and $VEGFR2^+$ cells among gated $CD31^+CD45^-$ ECs (4-5 mice/group in infected groups; 3 mice/group in PBS groups). *, $p < 0.05$; **, $p < 0.01$; and ***, $p < 0.001$; ****, $p < 0001$ compared to PBS controls. Graphs are shown as mean +/- SEM. Flow cytometric and qRT-PCR data were analyzed by using one-way ANOVA with Tukey's Post Hoc. At least 4 independent mouse infection experiments and 2 independent *in vitro* experiments were performed with similar trends, and shown are representative data.

Fig 2. Elevated Ang2 expression and decreased Ang1 expression during *O. tsutsugamushi* infection. Mice were infected as in *Fig. 1*. (A) Frozen lung sections were co-stained for Ang1 (a marker for endothelial quiescence, green), Ang2 (an endothelial stress marker, red), and DAPI

(blue) showing images at a low magnification (top row, scale bar = 50 μm) and close-up views of the boxed areas (bottom row, bar = 20 μm). (B) Quantification of fluorescent Ang1 and Ang2 staining (four images per time point). (C) Human serum Ang2 proteins in the control subjects (CNT) or scrub typhus patients (8/group) with different anti-*Orientia* IFA antibody titers were measured by ELISA. Shown are data from two independent experiments. *, $p < 0.05$; **, $p < 0.01$ and ***, $p< 0.001$; ****; $p < 0001$ compared to the controls. Graphs are shown as mean +/- SEM. Serum ELISA and qRT-PCR groups were analyzed via one-way ANOVA with Tukey's Post Hoc. At least 3 independent mouse infection experiments were performed with similar trends, and shown are representative data.

Fig 3. Reduced Tie2 expression and activation in the lungs of *O. tsutsugamushi* infected mice. Frozen lung tissue sections were stained for the Tie2 receptor (red) and DAPI (blue, bar = 50 μm). (B) Lung tissue homogenates (40 μg/lane) were measured by Western blots for the levels of phospho-Tie2 (pTie2) and total Tie2 proteins and compared with the GAPDH controls. (C) *TIE2* mRNA levels in mouse lungs were measured via qRT-PCR; data are presented as relative mRNA values normalized to GAPDH. **, $p < 0.01$ compared to the controls. Graph shown as mean +/- SEM. Serum ELISA and qRT-PCR groups were analyzed via one-way ANOVA with Tukey's Post Hoc.

Fig 4. Polarized MΦ activation in infected mouse lungs. Mice were infected with *O. tsutsugamushi* (4-5 mice/group) or PBS (3-4 mice/group) for lung tissues collection at indicated days of infection, as in *Fig. 1*. (A) Flow cytometric analyses of lung-derived cells, gated on $CD11b^{+}Ly6G^{-}$ MΦs and MΦ subsets, are shown for the D9 samples. The percentages and total numbers of (B) activated MΦs ($CD64^{+}CD11b^{+}Ly6G^{-}$), (C) M1-type MΦs

898 ($CD80^+CD64^+CD11b^+Ly6G^-$), as well as (D) M2-type MΦs ($CD206^+CD64^+CD11b^+Ly6G^-$) are
899 shown, respectively.

900 **Fig 5. Transcription of M1 and M2 associated genes in the lung of infected mice.** Lung
901 tissues were measured for the expression of M1-related genes (A) and M2-related genes (B),
902 respectively. Data are presented as relative to β-actin values. *, $p < 0.05$; **, $p < 0.01$; ***, $p <$
903 0.001 compared to the PBS controls. Graphs are shown as mean +/- SEM. One-way ANOVA
904 with Tukey's Post Hoc was used for statistical analysis. Two independent mouse infection
905 experiments were performed with similar trends, and shown are representative data.

906

907 **Fig 6. Enhanced bacterial growth in M2-polarized MΦs.** Bone marrow-derived MΦs were
908 generated from C57BL/6J mice, polarized into M1 or M2 types by pre-treatment of cells with
909 LPS (100 ng/ml) or rIL-4 (10 ng/ml), and infected with bacteria (5 MOI). (A) Bacterial loads at
910 3, 48, and 72 hpi (n = 5) were determined by qPCR. Data are presented as the *Orientia* 47-kDa
911 gene copy per pg of DNA. (B) Cells were co-stained for *Orientia* (green), IBA-1 (a MΦ marker,
912 red), and DAPI (blue) at 3 and 72 hpi. *, $p < 0.05$. Data for qPCR were analyzed via a Mann-
913 Whitney t test. Three independent experiments were performed with similar trends, and shown
914 are representative data.

915

916 ## Supporting information

917 **S1 Fig. Pulmonary pathology progression and reduced expression of occludin tight**
918 **junction proteins in infected lung tissues.** Female C57BL/6J mice (4-6 mice/group) were

inoculated with 1.325 x 10^6 of *O. tsutsugamushi* Karp strain. At indicated days of infection, equivalent lung portions were collected. (A) Hematoxylin and eosin staining of lung tissues during lethal challenge demonstrating increased cellular infiltration and alveolar thickening as the infection progresses (scale bars = 50 μm). (B) Frozen sections were processed for immunofluorescent staining and co-stained for occludin (cell-cell tight junctions, red), FITC-labeled GSL I-B_4 lectins (green, top rows, scale bars = 50 μm), and DAPI (blue). The close-up views of the boxed areas are shown in the lower row (bar = 20 μm). (C) Flow cytometry analysis of viable pulmonary ECs ($CD31^+CD45^-$) collected at early (D0) and late (D9) infection. (D) Cultured HUVECs were infected with bacteria at 3 or 10 multiplicity of infection (MOI, 4 samples/group) and analyzed via qRT-PCR for gene expression at 24 h post-infection. Data are presented as relative to GAPDH values. *, $p < 0.05$; **, $p < 0.01$; and ***, $p < 0.001$ compared to PBS controls. Graphs are shown as mean +/- SEM. Flow cytometric and qRT-PCR data were analyzed by using one-way ANOVA with Tukey's Post Hoc. At least 3 independent mouse infection experiments and 2 independent *in vitro* experiments were performed with similar trends, and shown are representative data.

S2 Fig. Leukocyte and T cell recruitment in the lungs of lethally challenged mice. Female C57BL/6J mice (3-5 mice per group) were inoculated with 1.325 x 10^6 of *O. tsutsugamushi* Karp strain. At indicated days of infection, equivalent lung portions were collected and processed for immunofluorescent staining or flow cytometric analysis. (A) Frozen sections were either co-stained for Ang2 (red) and CD45 (a leukocyte marker, green), or Ang2 (green) and CD3 (a T cell marker, red, bars = 50 μm). The percentage and absolute number of $CD3^+CD4^+$ T cells (B), as well as $CD3^+CD8^+$ T cells (C), were quantified and compared to non-infected controls

942 (*, $p<0.05$; **, $p<0.01$; ****, $p<0.0001$). Graphs are shown as +/- SEM. Flow cytometry groups
943 were analyzed using one-way ANOVA with Tukey's Post Hoc.

944

945 **S3 Fig. MΦ infection in mouse lungs and differentiation *in vitro*.** (A) Female C57BL/6J mice
946 (4-6 mice per group) were inoculated with 1.325 x 10^6 of *O. tsutsugamushi* Karp strain. At days
947 2 and 10, equivalent lung portions were processed; frozen sections were co-stained for *Orientia*
948 (red), IBA-1 (green, a macrophage marker), and DAPI (blue), showing images in a low-
949 magnification (top rows, scale bar = 50 μm) and close-up views of the boxed areas (bottom rows,
950 bar = 20 μm). (B) Bone marrow-derived MΦs were treated with LPS (100 ng/ml) or rIL-4 (10
951 ng/ml) for 24 h and analyzed for the expression of indicated markers via flow cytometry. The
952 numbers represent the percentages (%) of gated cells. (C) LPS- and IL-4-primed cells were
953 analyzed by qRT-PCR for the expression of the indicated markers, showing the polarization of
954 MΦ subsets compared with control cells (*, $p < 0.05$; **, $p < 0.01$; and ****, $p < 0.0001$). Data
955 are shown as +/- SEM and were analyzed using one-way ANOVA with Tukey's Post Hoc.

956 **S1 Table. Real-time PCR primers of human, murine, and bacterial genes.** The primer
957 sequences used in this study (listed in the 5' to 3' direction).

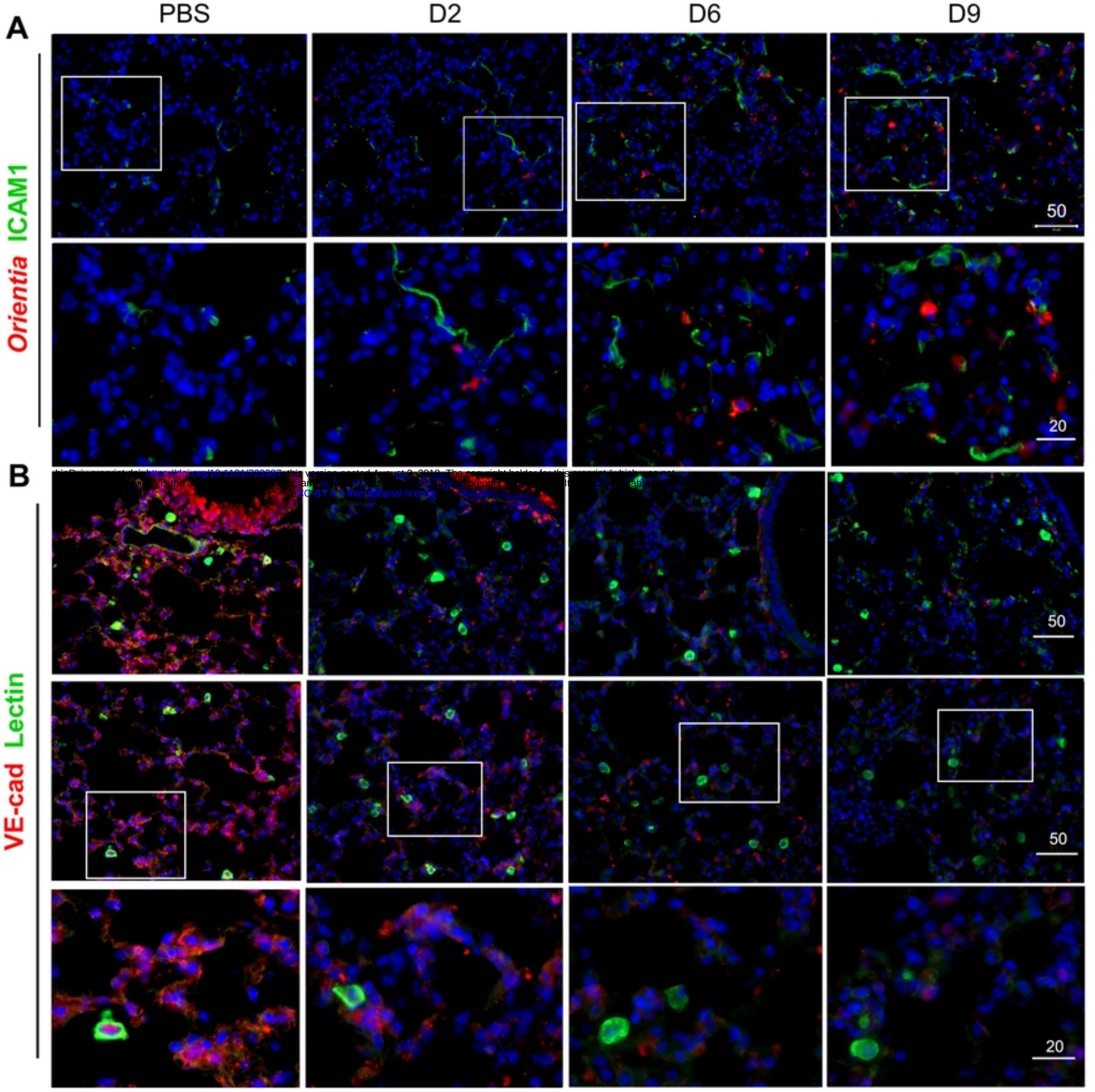

Figure 1

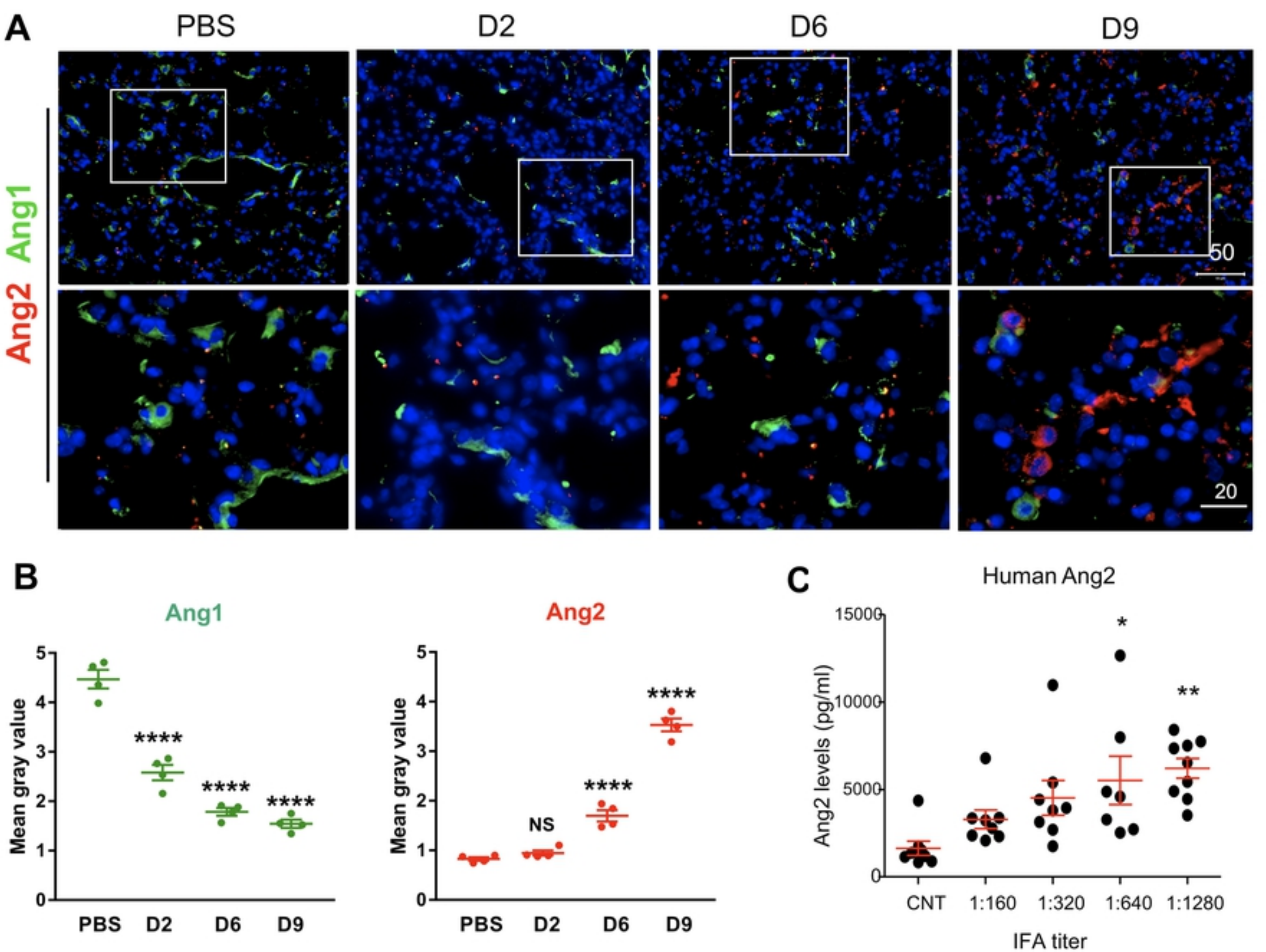
A
PBS
D2
D6
D9
Ang1
Ang2
50
20
B
Ang1
Mean gray value
5
4
3
2
1
0
****
****
****
PBS
D2
D6
D9
Ang2
Mean gray value
NS
****
****
C
Human Ang2
Ang2 levels (pg/ml)
15000
10000
5000
0
*
**
CNT
1:160
1:320
1:640
1:1280
IFA titer

Figure 2

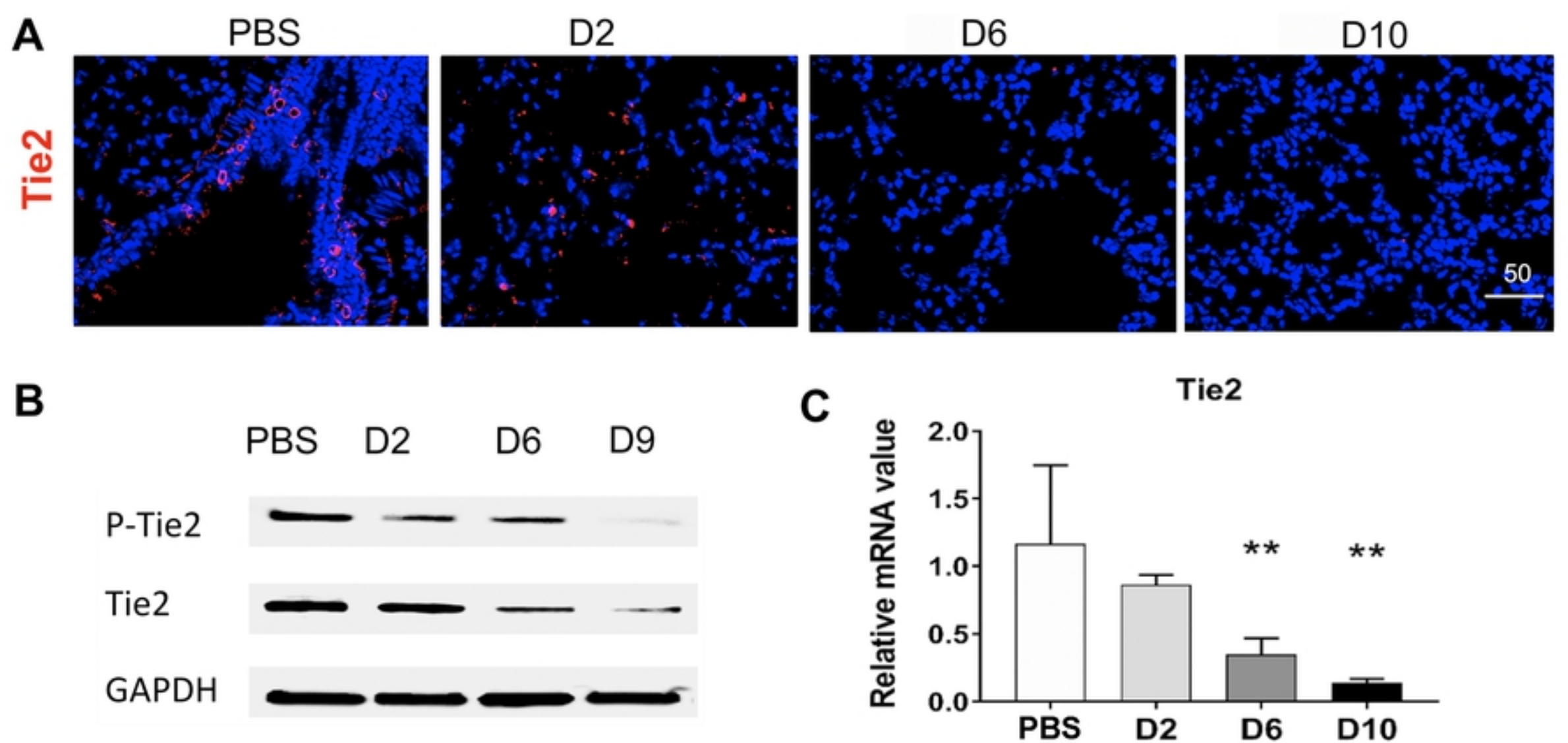
A
PBS
D2
D6
D10
Tie2
50
B
PBS
D2
D6
D9
P-Tie2
Tie2
GAPDH
C
Tie2
Relative mRNA value
2.0
1.5
1.0
0.5
0.0
**
**
PBS
D2
D6
D10

Figure 3

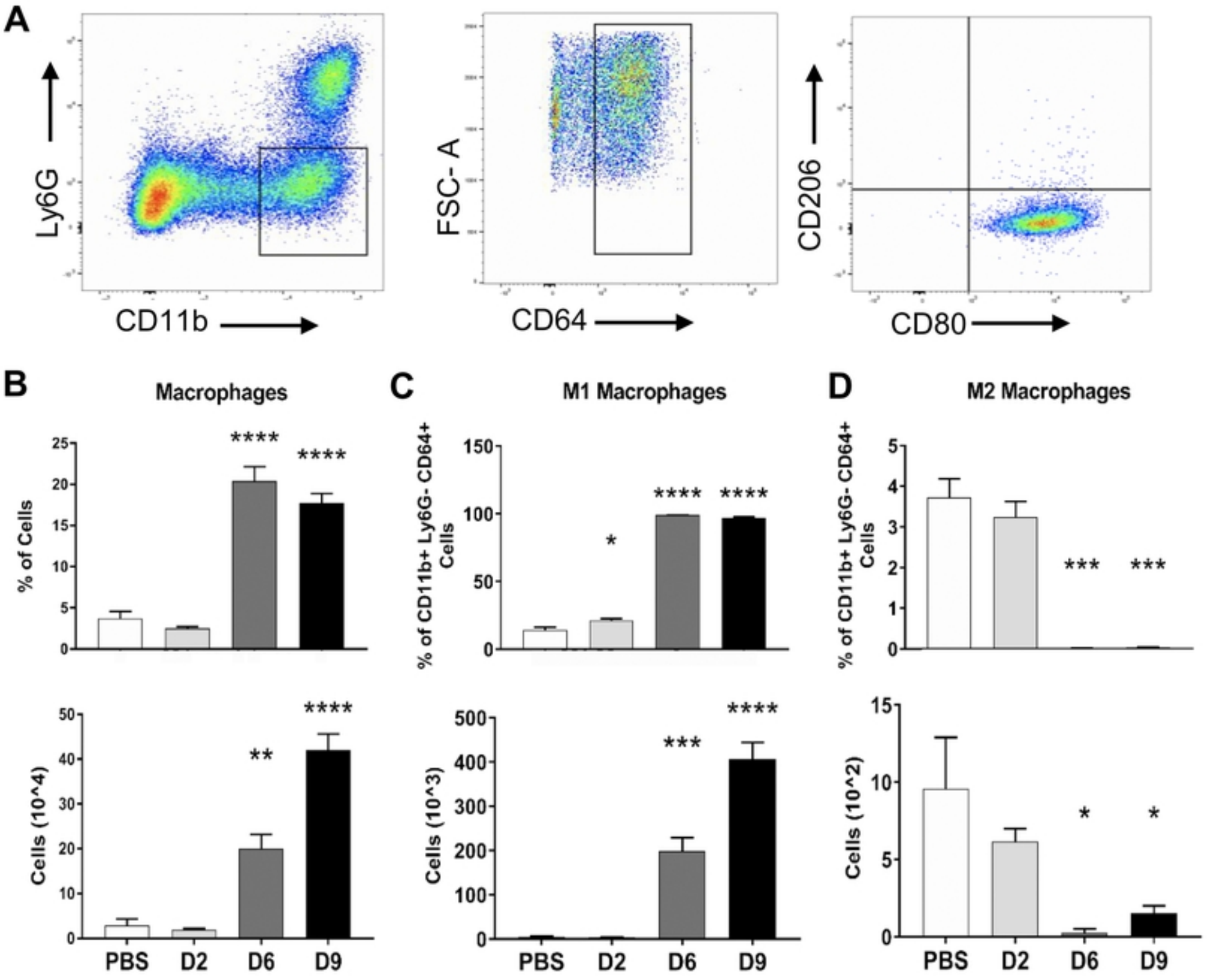
A
Ly6G
CD11b
FSC- A
CD64
CD206
CD80
B
Macrophages
% of Cells
Cells (10^4)
C
M1 Macrophages
% of CD11b+ Ly6G- CD64+ Cells
Cells (10^3)
D
M2 Macrophages
% of CD11b+ Ly6G- CD64+ Cells
Cells (10^2)
PBS
D2
D6
D9

Figure 4

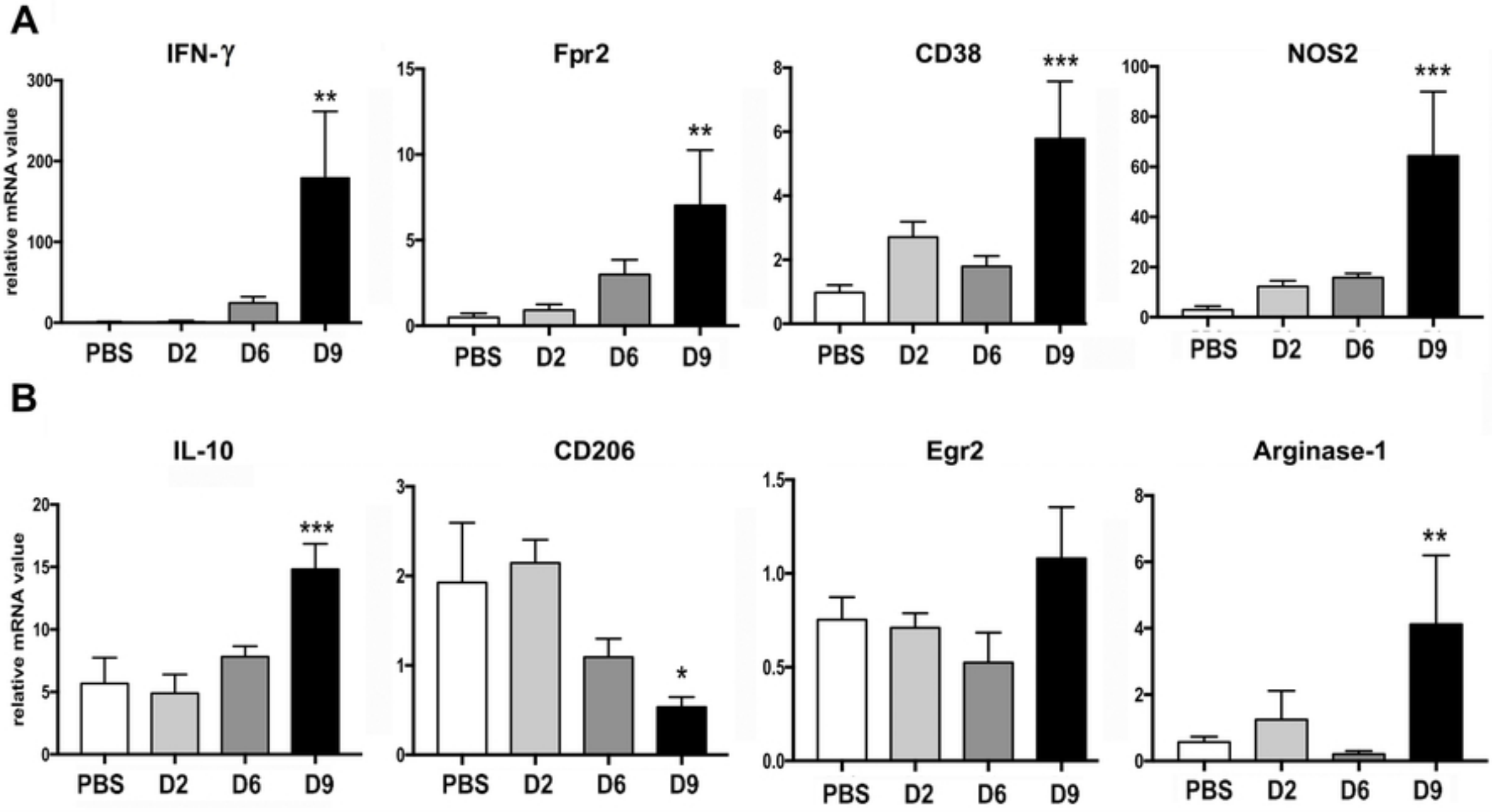
A
IFN-γ
Fpr2
CD38
NOS2
relative mRNA value
300
200
100
0
15
10
5
8
6
4
2
100
80
60
40
20
**
**
***
***
PBS
D2
D6
D9
B
IL-10
CD206
Egr2
Arginase-1
20
15
10
5
3
2
1
1.5
1.0
0.5
0.0
8
6
4
2
***
*
**

Figure 5

A

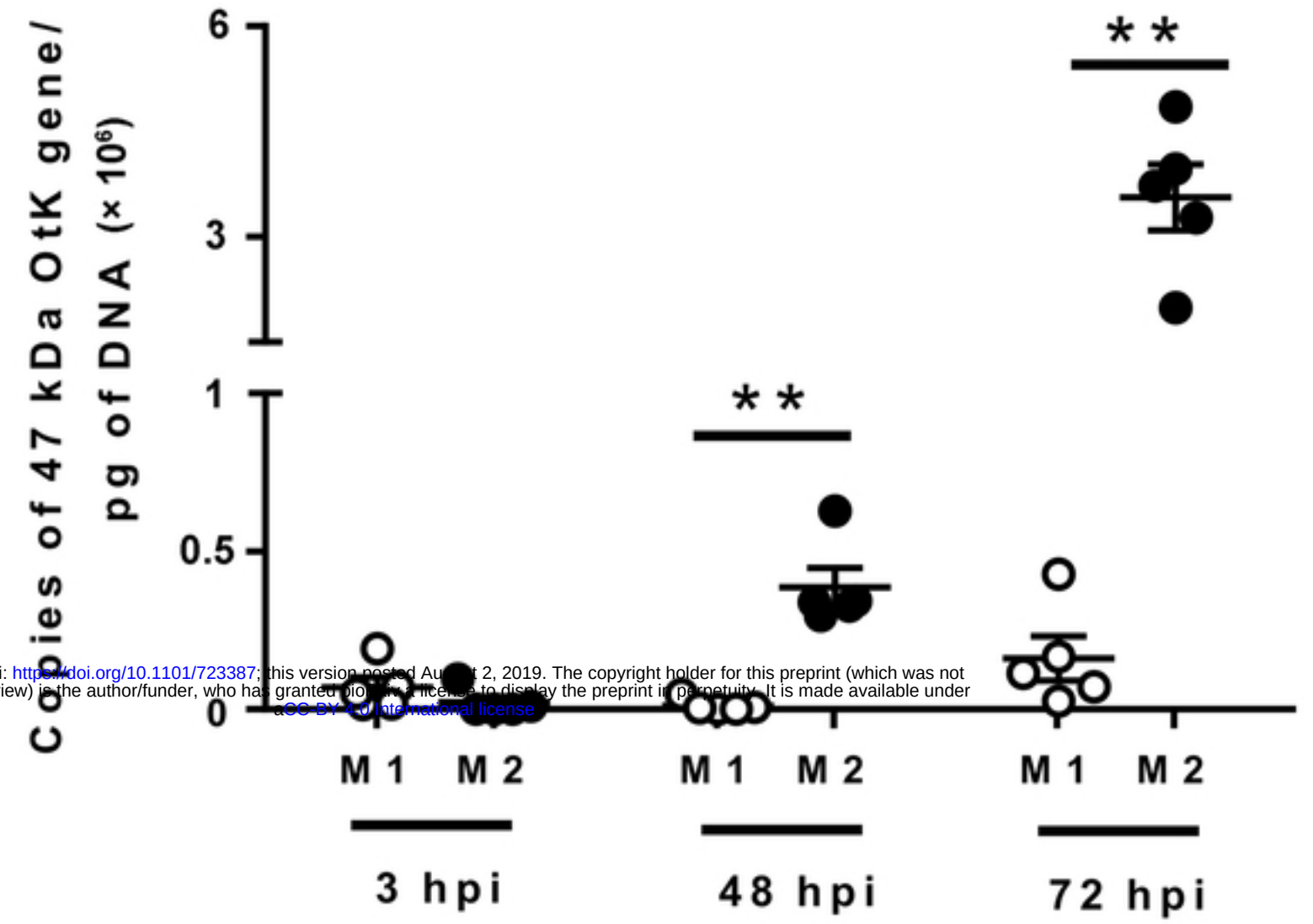

B

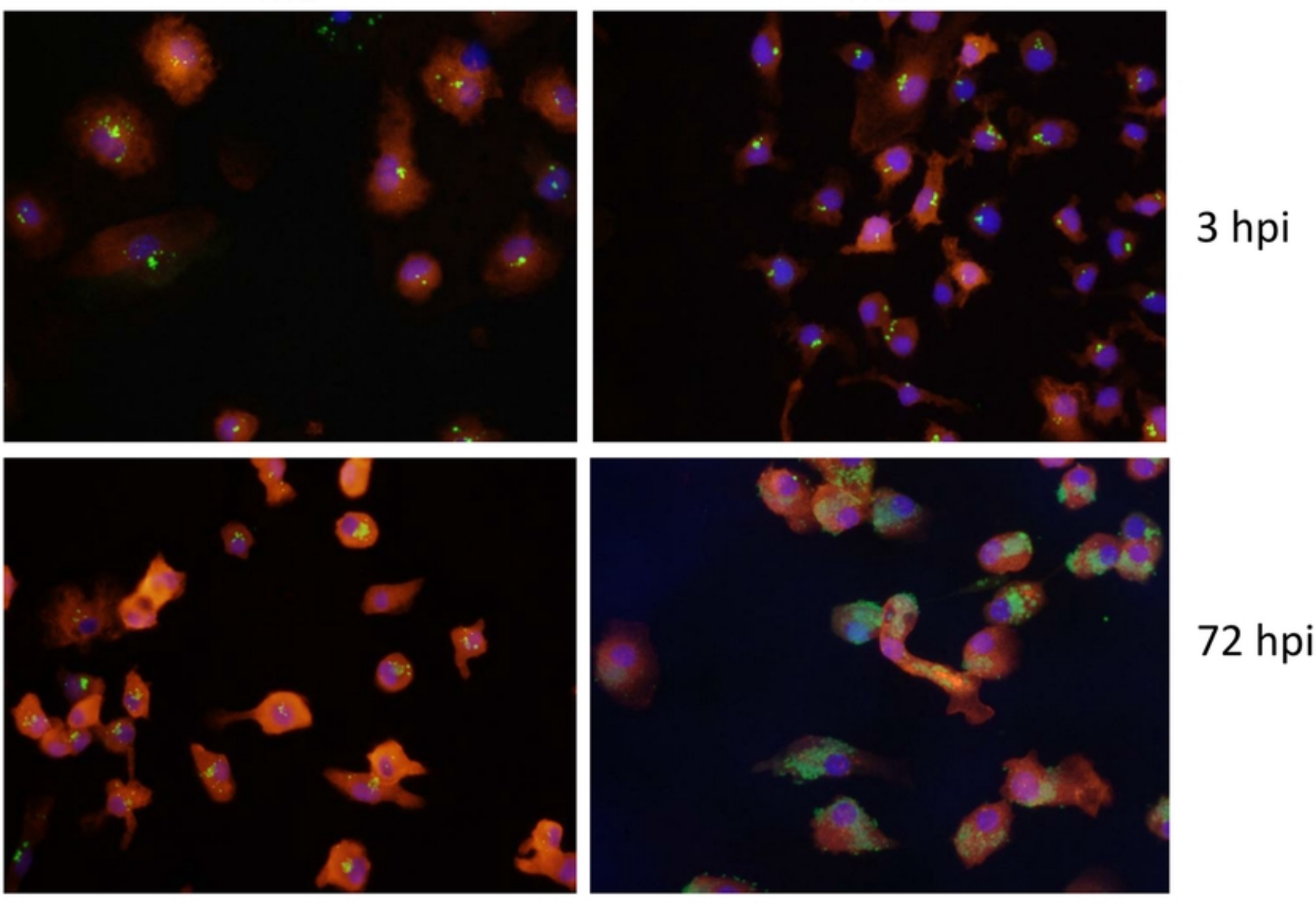

Figure 6

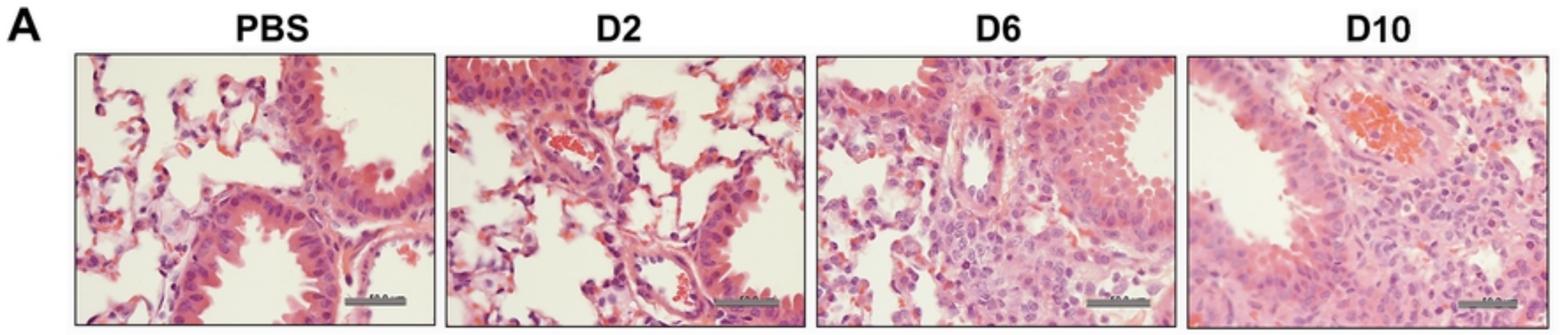

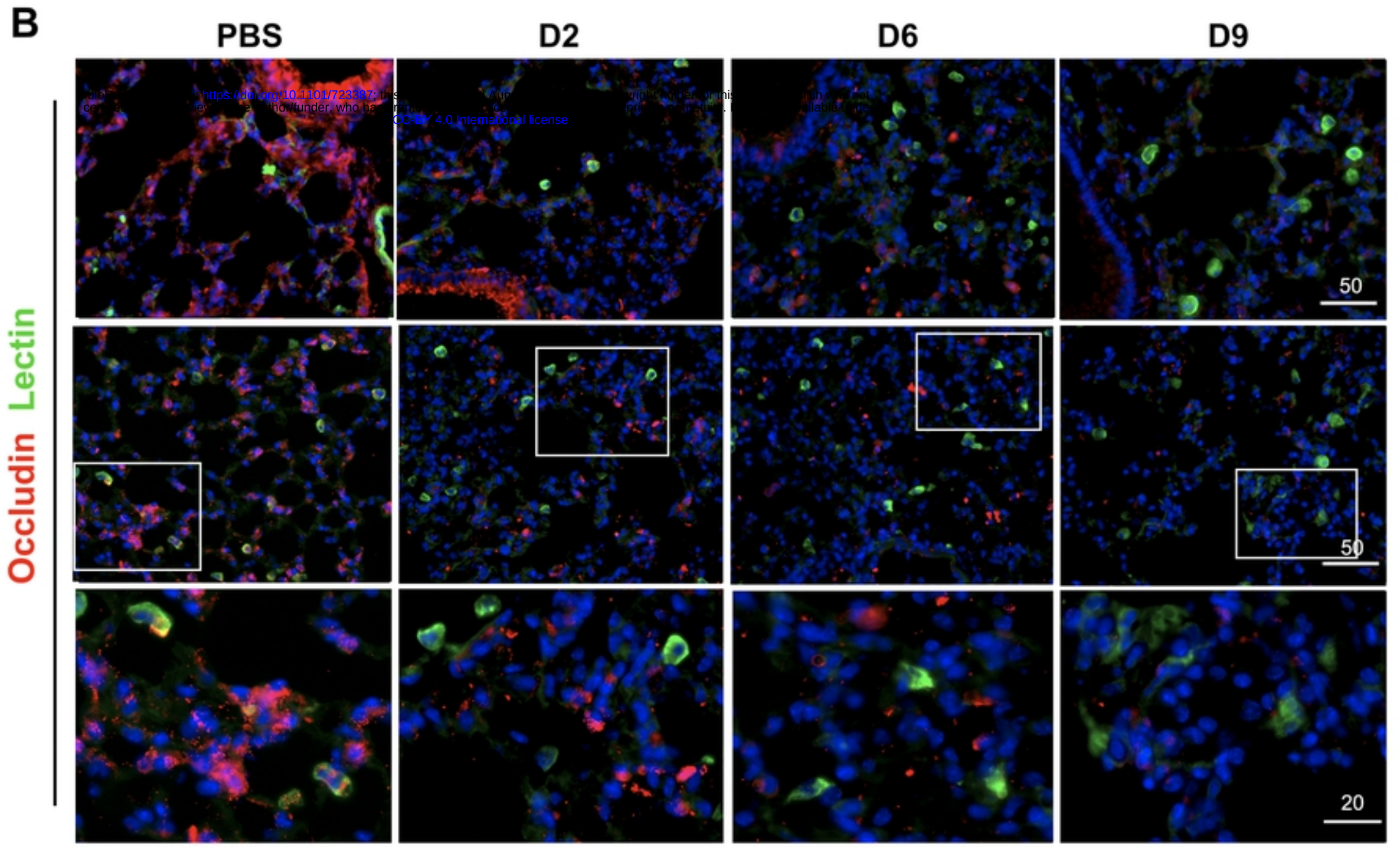

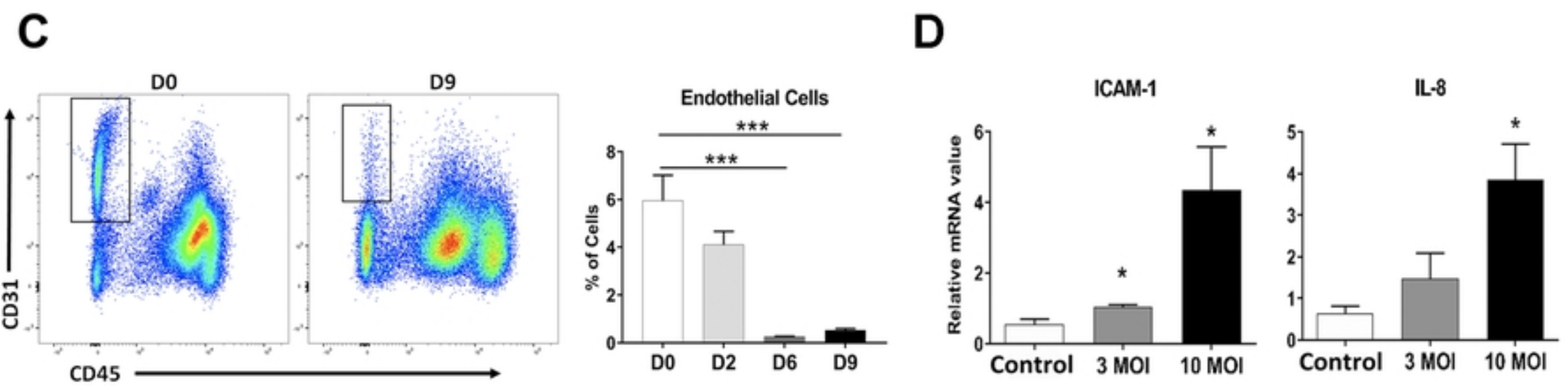

Figure S1

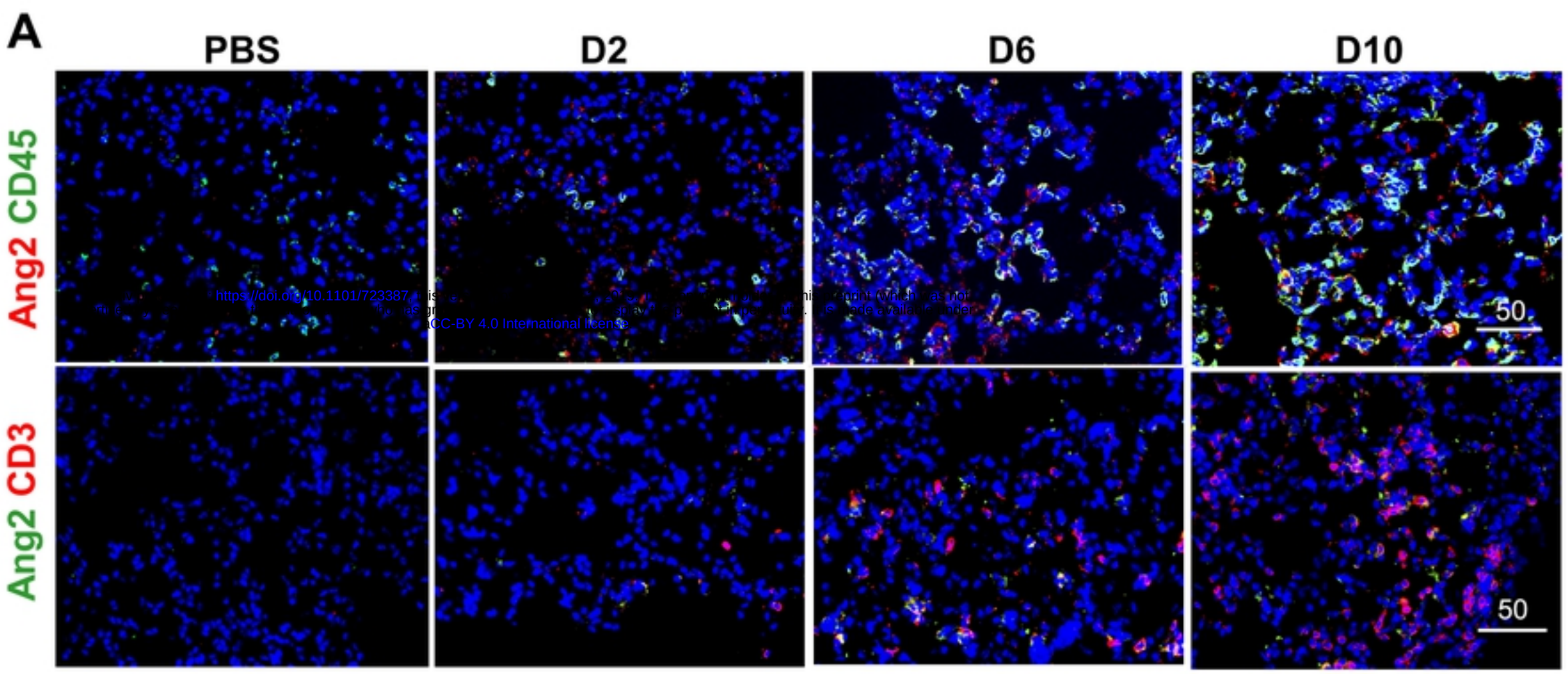

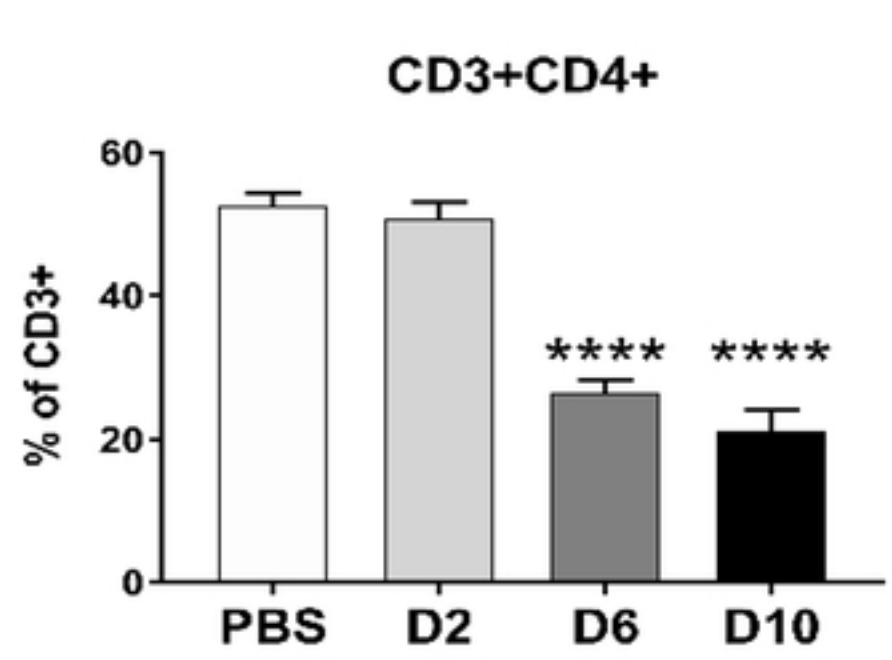

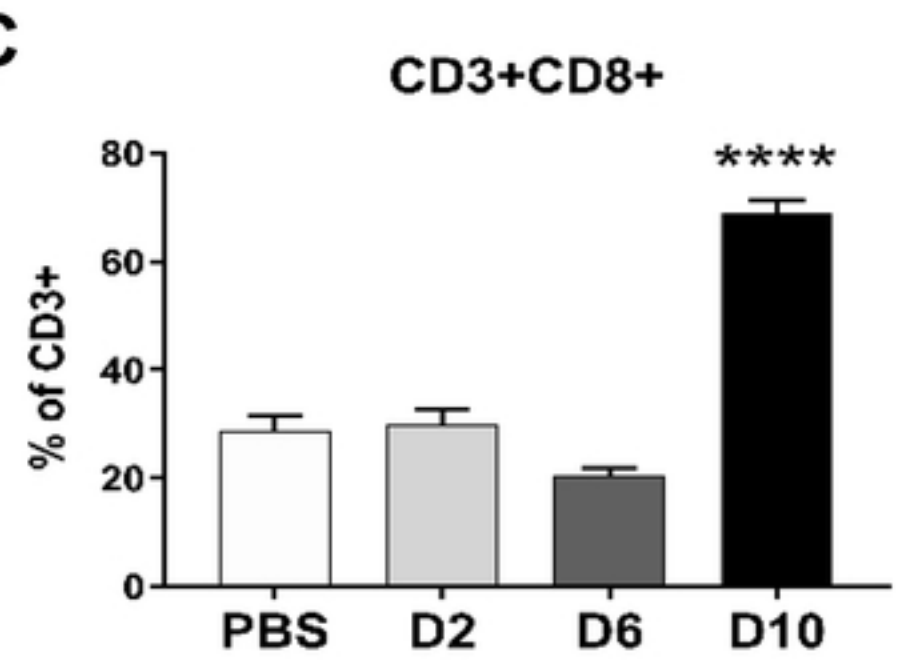

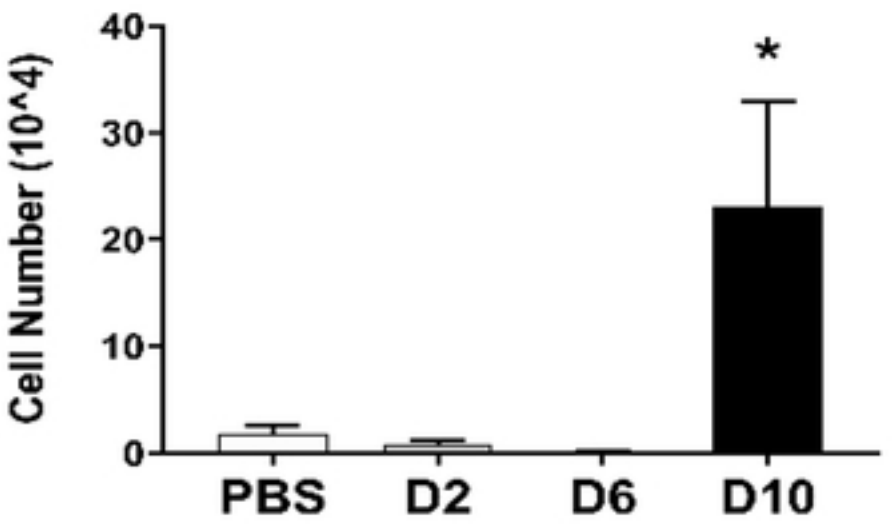

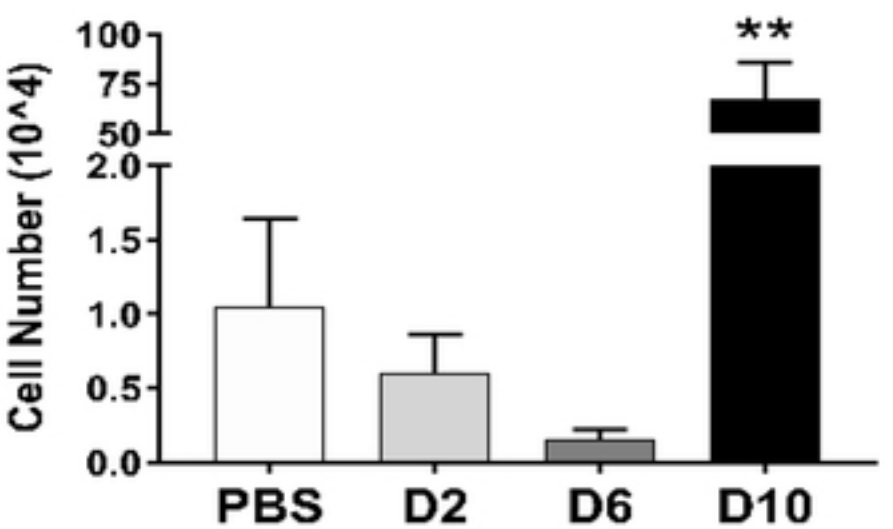

Figure S2

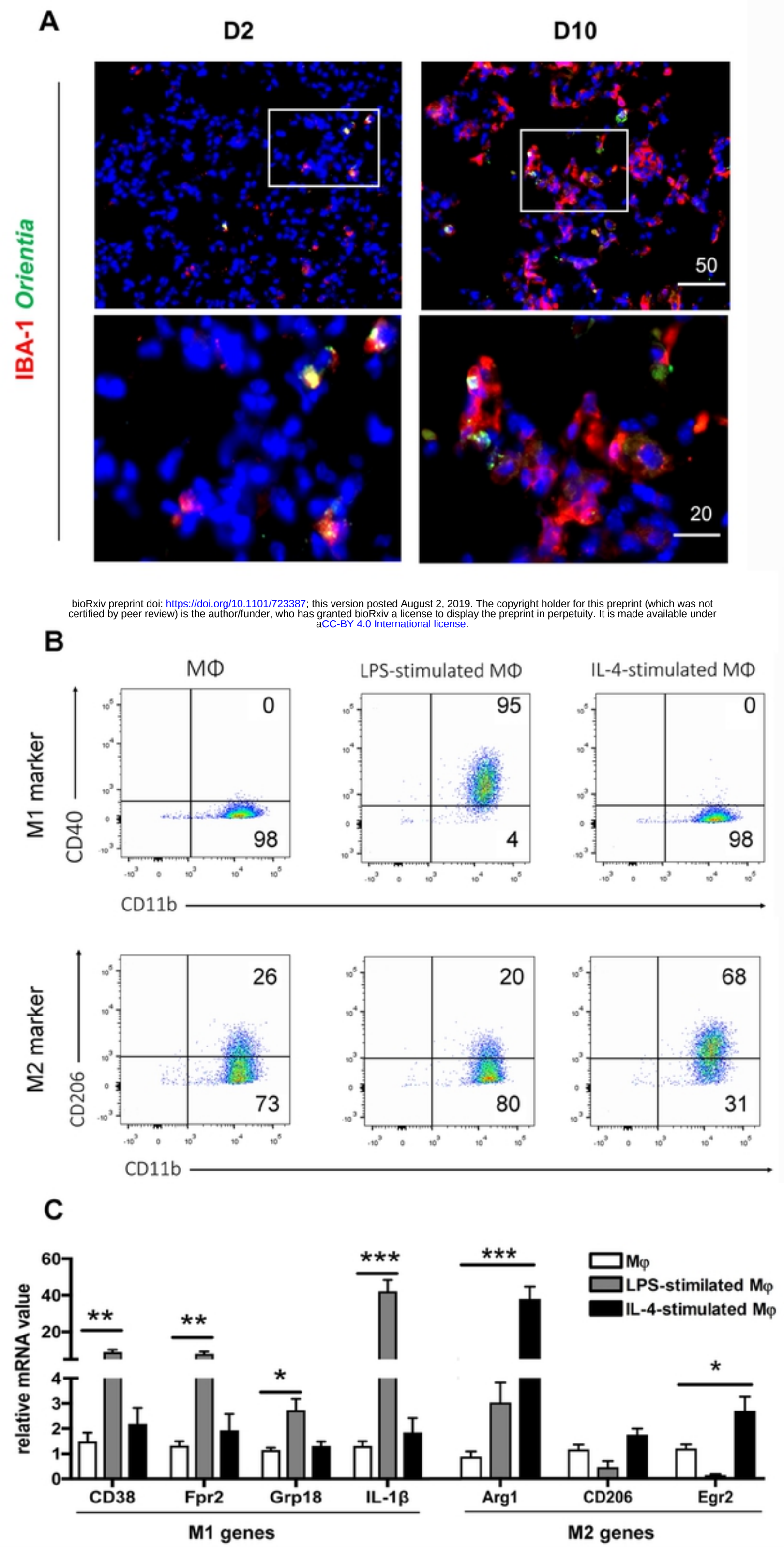

Figure S3